STAR-RIS-Empowered Cognitive Non-Terrestrial Vehicle Network with NOMA

Kefeng Guo, Rui Liu, Mamoun Alazab, *Senior Member, IEEE*, Rutvij H. Jhaveri, *Senior Member, IEEE*, Xingwang Li, *Senior Member, IEEE*, Mingfu Zhu

***Abstract*—In this paper, we investigate the outage behavior of a simultaneously transmitting and reflecting reconfigurable intelligent surface (STAR-RIS)-empowered cognitive non-terrestrial vehicle network with non-orthogonal multiple access (NOMA), in which Rician fading channels and imperfect/perfect successive interference cancellation (ipSIC/pSIC) are considered. In the network, STAR-RIS is utilized to assist the transmission and reflection of the superposed signals from a secondary unmanned aerial vehicle. Under the interference constraints of primary vehicle users, we derive the exact expressions of outage probability for all secondary vehicle users to evaluate the system parameters. Moreover, to gain deeper insights, the asymptotic expressions of outage probability along with the diversity order are obtained. Then, from numerical results, we confirm the correctness of our theoretical analysis and discuss the influences of key parameters on system performance. Compared with STAR-RIS-orthogonal multiple access (OMA)/non-STAR-RIS scheme, the superiority of our scheme is verified.**

***Index Terms*—Simultaneously transmitting and reflecting reconfigurable intelligent surface (STAR-RIS), cognitive non-terrestrial vehicle networks, non-orthogonal multiple access (NOMA), imperfect successive interference cancellation (ipSIC).**

I. Introduction

With the explosive growth of wireless communication demands, the next-generation wireless communication network should be characterized by high throughput, strong connectivity, high spectrum efficiency (SE), and seamless coverage [1], which cannot be achieved by traditional terrestrial network. Due to the extensive coverage, the non-terrestrial network has attracted the interest of many engineers and industrialists, which is regarded as a significant architecture in future wireless communication networks [2]–[4], especially for intelligent vehicle network. It can be predicted that the fixed spectrum allocation strategy and the rapid growth of the number of devices and vehicles will bring many challenges, thus we consider introducing cognitive radio (CR) and non-orthogonal multiple access (NOMA) into the non-terrestrial network to solve these problems [5]–[7]. In the complex urban environment, obstacle and fading will cause transmission interruption. Therefore, as a new disruptive technology, simultaneously transmitting and reflecting reconfigurable intelligent surface (STAR-RIS) is being intensively discussed, which can reflect and transmit the incident signals to devices/vehicles on both sides of it and expand coverage of the system [8]. Therefore, the integration of CR, NOMA, STAR-RIS, and non-terrestrial networks will tremendously improve the capability of existing wireless communication networks.

A. Related Works

Over recent years, the non-terrestrial network has been viewed as one of the candidates for the architecture of the future Internet of Things (IoT), Internet of Vehicles(IoV), which has the inherent characteristics of extensive coverage, long communication distance, flexible deployment, and so on [9]. A non-terrestrial network may consist of satellites, high altitude platforms (HAPs), unmanned aerial vehicles (UAVs), and vehicles, etc [10]–[12]. Besides, numerous works have been carried out to evaluate the performance of non-terrestrial networks [13]–[16]. The authors of [17] investigated the coverage probability and outage performance of a downlink satellite-aerial-terrestrial network, in which the end-to-end energy efficiency (EE) was maximized by jointly optimizing the transmit power and transmission time. In [18], the authors utilized successive convex approximation (SCA) method to design an alternating optimization beamforming scheme to enhance security and reduce energy consumption. A joint beamforming scheme was developed for a decode-and-forward relay assisted satellite-terrestrial network [19], in which the total transmit power of sources was minimized under the quality of service (QoS) constraints of users.

CR is widely discussed in the field of improving SE due to its dynamic utilization of spectrum [20]. At present, there are two main application modes: underlay and overlay. In underlay mode, the secondary network (SN) shares the spectrum of the primary network (PN) on the premise of ensuring the QoS of primary users (PUs) [21], [22]. It will inevitably

This work was supported by the National Natural Science Foundation of China under Grant 62001517, in part by the Key Scientific Research Projects of Higher Education Institutions in Henan Province under Grant 23B510001, in part by the Guangdong Basic and Applied Basic Research Foundation with grant number 2022A1515010999, in part by the Science and Technology Program of Guangzhou with grant number 202201011850, and in part by the Scientific Research Project of Education Department of Guangdong with grant number 2021KCXTD061. The corresponding author is Rui Liu (e-mail: lrevri@163.com).

K. Guo and R. Liu are with the School of Space Information, Space Engineering University, Beijing 101407, China (e-mail: guokefeng.cool@163.com, lrevri@163.com).

M. Alazab is with the Faculty of Science and Technology, Charles Darwin University, Casuarina, NT 0810, Australia (e-mail: alazab.m@ieee.org).

R. H. Jhaveri is with the Department of Computer Science and Engineering, School of Technology, Pandit Deendayal Energy University, Gandhinagar 382007, India (e-mail: rutvij.jhaveri@sot.pdpu.ac.in).

X. Li is with the School of Physics and Electronic Information Engineering, Henan Polytechnic University, Jiaozuo 454000, China (e-mail: lixingwangbupt@gmail.com).

M. Zhu is with the College of Computer Science and Technology, Henan Polytechnic University, Jiaozuo 454003, China (e-mail: zhumingfu@zzu.edu.cn).

cause interference to PN, but the system complexity is low [23]. In overlay mode, SN first negotiates with PN and gains the opportunity to access the authorized spectrum of PN by assisting PN in transmission [24], [25], which can enhance the system performance of PN. However, additional control links need to be established and more signaling overhead is required [26]. The authors of [27] discussed the reliable and secure performance of the cognitive ambient backscatter system, from which the outage probability (OP) and intercept probability (IP) were derived. In [28], a Dinkelbach and Lagrange-dual based scheme was designed to maximize the EE of a cognitive satellite-terrestrial network, where the outdated channel state information (CSI) and Poisson distributed terrestrial nodes were considered. The authors of [29] developed an iterative beamforming method to optimize the aggregated rate of the considered cognitive network, where the secrecy constraints and QoS demands were ensured.

With the growing demand for user connectivity, the traditional orthogonal multiple access (OMA) technology has gradually failed to meet the communication requirements of users [30], [31]. NOMA is considered as one of the candidates for the next-generation multiple access technology, which can allocate the same frequency/time/code to multiple users [32], [33]. Besides, the power domain NOMA has received a lot of attention[1], which implements spectrum multiplexing by installing successive interference cancellation (SIC) receivers at weak user ends [34]. Although the application of NOMA may lead to an increase in system complexity, its cost is shrinking with the maturity of industrial technology [35]. The authors of [36] jointly designed the NOMA precoding and UAV trajectory to optimize the transmission performance of the proposed UAV-NOMA network, where the interference elimination and interference limitation schemes were considered. In [37], the authors investigated the outage performance of the cache-free/cache-aided two-way relay NOMA assisted non-terrestrial network, where imperfect successive interference cancellation (ipSIC) was taken into consideration. The secrecy performance of a NOMA-based underlay cognitive non-terrestrial network with channel estimation errors and hardware impairments was analyzed in [38], in which the secrecy outage probability (SOP) and the secrecy energy efficiency (SEE) were obtained.

RIS is a passive digitally programmable planar, which has the advantages of low cost, high EE, and flexible deployment [39]. RIS can change the wireless propagation environment in real-time by adjusting the phase shift matrix [40], [41]. It is utilized to reflect signals from the source and enhance or weaken the incident signal according to demands, thus it can be applied to cooperative communication and enhance security [42], [43]. The authors of [44] designed a distributed and iterative algorithm to optimize the phase shift matrix and power allocation in the RIS-NOMA assisted simultaneous wireless information and power transfer (SWIPT) network. In [45], the authors utilized RIS to enhance the anti-jamming performance of the considered system with incomplete information. An alternative optimization scheme was developed to improve the SE and the security of multiuser networks [46]. However, RIS can only serve users on one side, and STAR-RIS makes up for this disadvantage, which can refract and reflect the incident signal simultaneously and provide more degree-of-freedom [47]. The authors of [48] investigated the secrecy performance of a STAR-RIS based NOMA system over Nakagami-m fading channels, in which the exact and asymptotic SOPs were derived. In [49], an energy splitting based block coordinate descent (BCD) scheme was developed to maximize the sum rate of the considered SATR-RIS empowered multiple-input multiple-output (MIMO) network, where the transmitting/reflecting factors and precoding matrices were jointly optimized. A path-following based beamforming and the transmitting/reflecting factors allocation scheme were designed to enhance the security of the considered system with STAR-RIS [50], in which energy allocation, mode selection, and time assignment were discussed.

B. Motivations and Contributions

As mentioned above, it is meaningful to study the performance of non-terrestrial vehicle networks with NOMA in the presence of interference constraints, in which CR and NOMA are introduced to improve SE, vehicle connectivity, and user fairness. At the same time, the appearance of STAR-RIS gives us more choices to improve coverage. As far as the author knows, CR, NOMA, or STAR-RIS has been studied in a few former works, but there is few work to apply STAR-RIS to the NOMA-based cognitive non-terrestrial vehicle network with ipSIC, which is mathematically complex and difficult to solve and motivates us to investigate it. In particular, the main contributions of our paper are presented in the following:

1) Considering the inherent advantages of CR, NOMA, and STAR-RIS, a STAR-RIS-empowered cognitive non-terrestrial vehicle network with NOMA is established, where the secondary UAV-vehicle network accesses the authorized spectrum of the primary satellite-vehicle network under the interference constraints of PUs. Besides, a pair of secondary users (SUs) form a NOMA group, and ipSIC is considered. On the foundation, STAR-RIS is utilized to transmit and reflect superposed signals to corresponding SUs over cascade Rician fading channels, respectively.
2) To evaluate the outage behavior of all SUs, the exact expressions of OP are derived by adopting Gauss-Chebyshev and Gauss-Laguerre quadratures. To analyze the system performance more clearly, we obtain the asymptotic OPs and diversity orders of strong vehicle user with ipSIC/pSIC and weak vehicle user at high signal-to-noise ratios (SNRs). For the purpose of comparison, the corresponding exact and asymptotic OPs of all SUs for STAR-RIS-OMA are also provided.
3) Simulation results are provided to verify our theoretical derivations. Moreover, we discuss the impacts of major parameters on outage performance in detail. Through comparison and analysis, it is confirmed that i) STAR-RIS can assist in transmission and enhance system throughput, ii) the outage behavior for STAR-RIS-NOMA outperforms that for STAR-RIS-OMA, iii) the

[1]In this paper, we mainly discuss the power domain NOMA. To simplify the expression, the NOMA mentioned below is the power domain NOMA

power allocation scheme and the number of configurable elements can be adjusted to satisfy the demands of users.

The remaining of this paper is shown in the following. The system model as well as problem formulation are established in Section II. In Section III, the investigations for the outage probability are provided. In Section IV, numerical results and performance evaluation of our proposed system are given. Finally, Section V summarizes the whole paper. **Notations:** $diag(\cdots)$ is the diagonal matrix, $(\cdot)^H$ stands for the conjugate-transpose, $J_n(\cdot)$ represents the first-kind Bessel function with order n, $\mathcal{CN}(\theta, \sigma^2)$ denotes the Gaussian distribution with mean θ and variance σ^2, $|\cdot|$ means the absolute value, $I_n(\cdot)$ is the n-order first-kind modified Bessel function, $E(\cdot)$ is the expectation, $D(\cdot)$ is the variance, $Q(\cdot,\cdot)$ stands for the generalized Marcum Q-function [51], $K_n(\cdot)$ is the n-order second-kind modified Bessel function [52, Eq. 8.432], $\Gamma(\cdot)$ is gamma function, and $\gamma(\cdot,\cdot)$ is the incomplete Gamma function [52, Eq. 8.350.1].

II. System Model and Problem Formulation

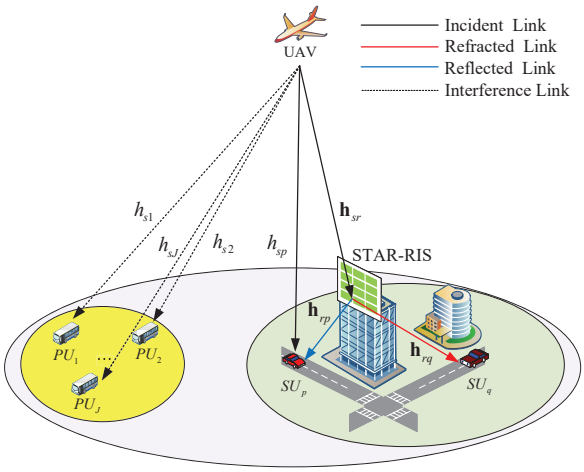

Fig. 1. System model

TABLE I
Symbol Meaning

notation	meaning
$P_s(W)$	transmit power of UAV
α_u	power allocation factor of SU_u
K	number of reflecting/transmitting elements
h_{sj}	channel coefficients of UAV-PU_j link
h_{sp}	channel coefficients of UAV-SU_p link
$\mathbf{h}_{sr}$	channel coefficients of UAV-STAR-RIS link
$\mathbf{h}_{ru}$	channel coefficients of STAR-RIS-SU_u link
Θ_R	reflecting phase shift matrix
Θ_T	transmitting phase shift matrix
$P_{max}(W)$	maximum transmit power of UAV
$I_{th}(W)$	interference threshold of PUs
β	Rician factor
V_{XY}	scaling factor indicating the actual propagation effects

As shown in Fig. 1, a STAR-RIS-empowered cognitive non-terrestrial vehicle network with NOMA is established, where a secondary UAV-vehicle network accesses the authorized spectrum of the primary satellite-vehicle network with the help of underlay CR. In particular, the PN consists of a satellite and multiple PUs $\{PU_j\}_{j=1}^{J}$, and a UAV as well as a pair of vehicle users $SU_u, u = \{p, q\}$ constitute the SN[2]. It is worth mentioning that the integrated signals $x(t) = \sqrt{\alpha_p P_s} x_p(t) + \sqrt{\alpha_q P_s} x_q(t)$ are transmitted and reflected to SU_u by adopting NOMA, where P_s is the transmit power of UAV, α_u denotes the power allocation factor of SU_u with $\alpha_p + \alpha_q = 1$. Due to the obstruction, we assume that there is no direct link between UAV and SU_q. Hence, the SU_q can only receive the signals refracted by STAR-RIS, while SU_p is able to obtain the signals from both UAV and STAR-RIS. In general, it is assumed that all sources and vehicles are equipped with broadband omnidirectional antennas[3] [33]. Besides, K reflecting elements and K refracting elements are assembled on STAR-RIS, which are utilized to reflect and refract the signals to vehicle users SU_p and SU_q respectively. Moreover, all channels experience Rician fading, and the channel coefficients of UAV-PU_j, UAV-SU_p, UAV-STAR-RIS, and STAR-RIS-SU_u links are denoted by h_{sj}, h_{sp}, $\mathbf{h}_{sr} \in \mathbb{C}^{K\times 1}$, and $\mathbf{h}_{ru} \in \mathbb{C}^{K\times 1}$ respectively. In this paper, we assume that perfect CSI is available,[4] and the imperfect CSI scenario will be extended in our future work. Furthermore, all nodes are interfered by additive white Gaussian noise (AWGN), which is modeled by $\mathcal{CN}(0, \sigma^2)$.

In addition, the reflecting and transmitting phase shift matrixs are represented by $\Theta_R = diag\left(\sqrt{\eta_1^r} e^{j\theta_1^r}, \sqrt{\eta_2^r} e^{j\theta_2^r}, \cdots, \sqrt{\eta_K^r} e^{j\theta_K^r}\right)$, and $\Theta_T = diag\left(\sqrt{\eta_1^t} e^{j\theta_1^t}, \sqrt{\eta_2^t} e^{j\theta_2^t}, \cdots, \sqrt{\eta_K^t} e^{j\theta_K^t}\right)$, where $\eta_k^r, \eta_k^t \in [0,1]$ and $\theta_k^r, \theta_k^t \in [0, 2\pi)$ are the amplitude factor and phase shift of k-th reflecting/transmitting elements. Thus the cascade channel gains of UAV-STAR-RIS-SU_p and UAV-STAR-RIS-SU_q links can be expressed as $\mathbf{h}_{sr}^H \Theta_R \mathbf{h}_{rp}$ and $\mathbf{h}_{sr}^H \Theta_T \mathbf{h}_{rq}$. To realize the STAR scheme, the mode-switching method proposed by [8] is adopted in our considered system. More specifically, for k-th reflective link, we set the amplitude factors $\eta_k^r = 1$ and $\eta_k^t = 0$, while for k-th transmitting link, we have $\eta_k^r = 0$ and $\eta_k^t = 1$.

Recalling the underlay CR, the QoS of PN must be ensured, thus the transmit power of UAV is limited by the interference constraint of PUs, i.e., $P_s = \min\left\{P_{max}, I_{th} / \max_{j=1,2,\cdots,J} |h_{sj}|^2\right\}$, where P_{max} is the maximum transmit power of UAV, and I_{th} is the interference threshold of PUs.

A. Signal Model

On the basis of the NOMA scheme, the vehicle user SU_p receives the superposed signals from UAV and SATR-RIS,

[2]The multiple-vehicle group will be investigated in our future work.

[3]For the goal of reduce the complexity and cost, the above assumption is made.

[4]The perfect CSI can be achieved by feedback/training processes.

thus the received signals of it can be expressed as

$$y_p(t) = \left(h_{sp} + \mathbf{h}_{sr}^H \Theta_R \mathbf{h}_{rp}\right) x(t) + n_p, \tag{1}$$

where n_p is AWGN.

Due to the obstacles, only signals transmitted by STAR-RIS can be observed by the vehicle user SU_q, which is shown as

$$y_q(t) = \left(\mathbf{h}_{sr}^H \Theta_T \mathbf{h}_{rq}\right) x(t) + n_q, \tag{2}$$

where n_q is AWGN.

Denoting $\mathbf{h}_{sr} = [h_{s1}, h_{s2}, \cdots, h_{sK}]^H$, and $\mathbf{h}_{ru} = [h_{1u}, h_{2u}, \cdots, h_{Ku}]^H$, where h_{sk} and h_{ku} are the channel coefficients from UAV to k-th reflecting/transmitting element, and from k-th reflecting/transmitting element to the vehicle user SU_u. According to the characteristics of Rician fading, the channel coefficient can be re-written as

$$h_{XY} = \sqrt{V_{XY}} \left(\sqrt{\frac{\beta}{\beta+1}} + \sqrt{\frac{1}{\beta+1}} \tilde{h}_{XY} \right), \tag{3}$$

where $X = \{s, r\}, Y = \{r, p, q\}$, $\tilde{h}_{XY} \sim \mathcal{CN}(0,1)$, and $V_{XY} = G_{s,Y} \varepsilon_u \kappa_{XY}$ is a scaling factor indicating the actual propagation effects. Firstly, G_s denotes the transmitting antenna gain of UAV, which is given by

$$G_{s,Y} = G_{s,\max} \left[\frac{J_1(t_Y)}{2t_Y} + 36 \frac{J_3(t_Y)}{t_Y^3} \right]^2, \tag{4}$$

where $G_{s,\max}$ represents the maximal transmitting antenna gain of the UAV, $t_Y = 2.70123 \sin \varpi_Y / \sin \varpi_{Y,3dB}$ with ϖ_Y standing for the angle between UAV and Y and $\varpi_{Y,3dB}$ being 3-dB angel. Besides, ε_u is the receiving antenna gain of SU_u, which can be expressed as

$$\varepsilon_u = \begin{cases} \varepsilon_{u,\max} - 2.5 \times 10^{-3} \left(\frac{d_u \vartheta}{\lambda}\right)^2, & 0^\circ < \vartheta < \vartheta_1 \\ 2 + 15 \log \frac{d_u}{\lambda}, & \vartheta_1 < \vartheta < \vartheta_2 \\ 32 - 25 \log \vartheta & \vartheta_2 < \vartheta < 48^\circ \\ -10 & 48^\circ < \vartheta < 180^\circ \end{cases}, \tag{5}$$

where $\varepsilon_{u,\max}$ denotes the maximal receiving antenna gain of SU_u, d_u represents the receiving antenna diameter of SU_u, λ stands for wavelength, ϑ denotes the angle of off-boresight, $\vartheta_1 = \frac{20\lambda}{d_Y} \sqrt{\varepsilon_{u,\max} - \left(2 + 15 \log \frac{d_u}{\lambda}\right)}$ and $\vartheta_2 = 15.85 \left(\frac{d_u}{\lambda}\right)^{-0.6}$. Furthermore, κ_{XY} indicates the effects of free-space loss (FSL) with

$$\kappa_{XY} = \frac{v^2}{f^2 \left(d_{XY}^2 + d_X^2\right)}, \tag{6}$$

where $v = c/4\pi$ with c denoting the speed of light, f stands for the carrier frequency, d_{XY} shows the distance from the center of the coverage area for UAV to STAR-RIS and secondary vehicle users, and d_X is the relative height of UAV/RIS.

Moreover, we assume that $\alpha_p < \alpha_q$, thus the SIC receiver is configured on SU_p. In particular, SU_p decodes the signal of SU_q, then the decoded signal is eliminated from the superposed signal and SU_p detects its signal x_p.

Therefore, the signal-plus-interference-to-noise ratio (SINR) of x_q at SU_p is represented as

$$\gamma_{p \to q} = \frac{\alpha_q \rho_s \left| h_{sp} + \mathbf{h}_{sr}^H \Theta_R \mathbf{h}_{rp} \right|^2}{\alpha_p \rho_s \left| h_{sp} + \mathbf{h}_{sr}^H \Theta_R \mathbf{h}_{rp} \right|^2 + 1}, \tag{7}$$

where $\rho_s = P_s / \sigma^2$ denotes the average SNR. Next, the SINR of x_p at SU_p is given by

$$\gamma_p = \frac{\alpha_p \rho_s \left| h_{sp} + \mathbf{h}_{sr}^H \Theta_R \mathbf{h}_{rp} \right|^2}{\omega \rho_s \left| h_{ip} \right|^2 + 1}, \tag{8}$$

where $h_{ip} \sim \mathcal{CN}(0, \Omega_{ip})$ is the residual interference due to ipSIC, and $\omega = 0/1$ stands for the pSIC/ipSIC case.

For SU_q, only its own signal needs to be decoded, and the signal of SU_p is regarded as interference, thus the SINR at SU_q can be expressed as

$$\gamma_q = \frac{\alpha_q \rho_s \left| \mathbf{h}_{sr}^H \Theta_T \mathbf{h}_{rq} \right|^2}{\alpha_p \rho_s \left| \mathbf{h}_{sr}^H \Theta_T \mathbf{h}_{rq} \right|^2 + 1}. \tag{9}$$

B. STAR-RIS-OMA

In this subsection, we investigate the OMA-based system which can be taken as the comparison benchmark of our proposed system. Moreover, STAR-RIS is also utilized to assist the transmission from the UAV to secondary vehicle users. On this foundation, the SINRs at SU_p and SU_q in STAR-RIS-OMA case are represented as, respectively,

$$\gamma_p^{OMA} = \rho_s \left| h_{sp} + \mathbf{h}_{sr}^H \Theta_R \mathbf{h}_{rp} \right|^2, \tag{10}$$

and

$$\gamma_q^{OMA} = \rho_s \left| \mathbf{h}_{sr}^H \Theta_T \mathbf{h}_{rq} \right|^2. \tag{11}$$

C. Channel Statistical Properties

To investigate the outage performance, the channel statistical properties of all channels must be given. Only two kinds of channels exist in our proposed system, namely, the Rician channel and the cascade Rician channel. Firstly, according to [53], the probability distribution function (PDF) and cumulative distribution function (CDF) of $|h_{XY}|$ are given by, respectively,

$$f_{|XY|}(x) = \frac{2x(\beta+1)}{V_{XY} e^\beta} e^{-\frac{x^2(\beta+1)}{V_{XY}}} I_0 \left(2x \sqrt{\frac{\beta(\beta+1)}{V_{XY}}} \right), \tag{12}$$

and

$$F_{|XY|}(y) = 1 - Q\left(\sqrt{2\beta}, y \sqrt{\frac{2(\beta+1)}{V_{XY}}} \right). \tag{13}$$

In this paper, the coherent phase shifting scheme is selected to obtain excellent performance of cascade Rician channels, in which the transmitting/reflecting phase shift matrix of STAR-RIS can match the phase shift of channels. Let $X_u^k = \left| h_{sr}^k h_{ru}^k \right|$, with the help of [54], we can obtain the PDF of cascade Rician

channels as

$$f_{X_u^k}(x) = \frac{1}{\sqrt{V_{sr}V_{ru}}} \sum_{i=0}^{\infty}\sum_{j=0}^{\infty} (V_{sr}V_{ru})^{-\frac{i+j+1}{2}} \times \frac{4x^{i+j+1}(\beta+1)^{i+j+2}\beta^{i+j}}{(i!)^2(j!)^2 e^{2\beta}} K_{i-j}\left[2x(\beta+1)\right]. \tag{14}$$

Denoting the mean and variance of X_u^k by μ_u and Ω_u, which are shown as, respectively,

$$\mu_u = E\left(X_u^k\right) = \frac{\pi\sqrt{V_{sr}V_{ru}}}{4(\beta+1)}\left[L_{1/2}(-\beta)\right]^2, \tag{15}$$

and

$$\Omega_u = D\left(X_u^k\right) = V_{sr}V_{ru} - \frac{\pi^2 V_{sr}V_{ru}}{16(\beta+1)^2}\left[L_{1/2}(-\beta)\right]^4, \tag{16}$$

where $L_{1/2}(-\beta) = e^{\frac{1}{2}}\left[(1+\beta)K_0\left(\frac{\beta}{2}\right) + \beta K_1\left(\frac{\beta}{2}\right)\right]$ stands for the Laguerre polynomial.

III. Outage Probability Analysis

In this section, we investigate the outage performance of the STAR-RIS-empowered cognitive non-terrestrial vehicle network with NOMA. In particular, the exact OPs of SU_p with ipSIC/pSIC and SU_q are obtained, respectively. For the purpose of comparison, we also provide the OP of secondary vehicle users in STAR-RIS-OMA case. To get further insights, the asymptotic OPs and diversity orders are derived.

A. OP of vehicle user SU_p

As mentioned above, SU_p adopts SIC to decode signals. Hence, if the signal x_p or x_q is detected unsuccessfully, the interruption occurs. Then the OP of SU_p is given by

$$P_p = \Pr\left(\gamma_{p\to q} < \gamma_q^{th}\right) + \Pr\left(\gamma_p < \gamma_p^{th}\right) - \Pr\left(\gamma_p < \gamma_p^{th}\right)\Pr\left(\gamma_{p\to q} < \gamma_q^{th}\right) \tag{17}$$

where $\gamma_q^{th} = 2^{R_q^{th}} - 1$ and $\gamma_p^{th} = 2^{R_p^{th}} - 1$ stand for SNR thresholds of SU_p and SU_q, R_q^{th} and R_p^{th} represent rate thresholds of corresponding secondary vehicle users. On this foundation, the exact OP of SU_p is given as follows.

Theorem 1. *When $\omega = 1$, the exact OP of SU_p with ipSIC can be expressed as*

$$P_{p,ipSIC} = Q_{p,1} + Q_{p,2} + Q_{p,3} + Q_{p,4} - Q_{p,1}Q_{p,2} - Q_{p,3}Q_{p,4}, \tag{18}$$

where $Q_{p,1}$, $Q_{p,2}$, $Q_{p,3}$, and $Q_{p,4}$ are given by (19), (20), (21), *and* (22), $\tau_{1,1} = \frac{\gamma_q^{th}}{\rho_{\max}\left(\alpha_q - \gamma_q^{th}\alpha_p\right)}$, $\tau_{2,1} = \frac{\gamma_p^{th}}{\rho_{\max}\alpha_p}$, $\tau_{1,2} = \frac{\gamma_q^{th}}{\rho_{th}\left(\alpha_q - \gamma_q^{th}\alpha_p\right)}$, $\tau_{2,2} = \frac{\gamma_p^{th}}{\rho_{th}\alpha_p}$, $\varphi_p = \frac{\mu_p^2 K - \Omega_p}{\Omega_p}$, $\phi_p = \frac{\Omega_p}{\mu_p}$, $\xi = \frac{\rho_{th}}{\rho_{\max}}$, $\Lambda_n = \frac{\pi}{(2\phi_p)^{\varphi_p+1}T_n\Gamma(\varphi_p+1)}$, $n = \{1,2,3,4\}$, $\Phi_l = \frac{(x_l+1)\xi}{2}$, $l = \{e,h,t_n\}$, $x_l = \cos\left(\frac{2l-1}{2L}\pi\right)$, $L = \{E,H,T_n\}$ *is the Chebyshev tradeoff factor,* $H_w = \frac{y_w}{[(w+1)L_{w+1}(y_w)]^2}$, $L_{w+1}(y_w) = \sum_{b=0}^{w+1}\binom{w+1}{b}\frac{(-1)^b}{b!}y_w^b$ *is the Laguerre polynomial with $w = \{p, p_2\}$ as the Laguerre tradeoff factor, y_w is the l-th zero point, and $\Phi = \sqrt{\tau_{2,1}(\omega\rho_{\max}y_p\Omega_{ip}+1)}$.*

Proof: Please see Appendix A. ■

Theorem 2. *When $\omega = 0$, the exact OP of SU_p with pSIC can be expressed as*

$$P_{p,pSIC} = Q_{p,5} + Q_{p,6} - Q_{p,5}Q_{p,6}, \tag{23}$$

where $Q_{p,5}$, $Q_{p,6}$ are given by (24), (25), $\tau_1 = \max(\tau_{1,1}, \tau_{2,1})$, $\tau_2 = \max(\tau_{1,2}, \tau_{2,2})$, $\Phi_r = \frac{(x_r+1)\xi}{2}$, $r = \{e_2, t_5, t_6\}$, $x_r = \cos\left(\frac{2r-1}{2R}\pi\right)$, $R = \{E_2, T_5, T_6\}$ *is the Chebyshev tradeoff factor.*

Proof: With some integral transformations, the CDF of Ξ_R can be re-written as

$$F_{\Xi_R}(\Xi_R) = \sum_{t_1=0}^{T_1} \frac{\pi\Xi_R(\beta+1)\sqrt{1-x_{t_1}^2}}{2T_1V_{sp}e^{\beta}\Gamma(\varphi_p+1)}(1+x_{t_1}) \times e^{-\frac{\tau_1\left(1+x_{t_1}\right)^2(\beta+1)}{4V_{sp}}} I_0\left((1+x_{t_1})\sqrt{\frac{\Xi_R\beta(\beta+1)}{V_{sp}}}\right) \times \gamma\left(\varphi_p+1, \frac{\sqrt{\Xi_R}(1-x_{t_1})}{2\phi_p}\right). \tag{26}$$

With the help of (26), similar to the derivation processes of $Q_{p,1}$ and $Q_{p,3}$ in Appendix A, Theorem 2 can be proved. To simplify the expression, the specific steps are omitted here. ■

B. OP of vehicle user SU_q

SU_q only detects its desired signal x_q, thus there is no ipSIC case for it. Then, the exact expression of OP for SU_q can be expressed as

$$P_q = \Pr\left(\gamma_q < \gamma_q^{th}\right). \tag{27}$$

Theorem 3. *Considering the Rician fading, we can obtain the exact OP of SU_p as*

$$P_q = 1 - \frac{1}{\Gamma(\varphi_q+1)}\left\{\sum_{u_1=0}^{U_1}\sqrt{1-x_{u_1}^2}\frac{J(\beta+1)}{V_{sj}e^{\beta}}e^{-\frac{\Phi_{u_1}(\beta+1)}{V_{sj}}} \times \frac{\pi\xi}{2U_1}\gamma\left(\varphi_q+1, \frac{\sqrt{\tau_{1,2}\Phi_{u_1}}}{\phi_q}\right) I_0\left(2\sqrt{\frac{\Phi_{u_1}\beta(\beta+1)}{V_{sj}}}\right) \times \left[1 - Q\left(\sqrt{2\beta}, \sqrt{\frac{2\Phi_{u_1}(\beta+1)}{V_{sj}}}\right)\right]^{J-1} + \sum_{j=0}^{J}\binom{J}{j} \times (-1)^j\left[Q\left(\sqrt{2\beta}, \sqrt{\frac{2\xi(\beta+1)}{V_{sj}}}\right)\right]^j \gamma\left(\varphi_q+1, \frac{\sqrt{\tau_{1,1}}}{\phi_q}\right)\right\}, \tag{28}$$

where $\Phi_{u_1} = \frac{(x_{u_1}+1)\xi}{2}$, $x_{u_1} = \cos\left(\frac{2u_1-1}{2U_1}\pi\right)$, and U_1 is the Chebyshev tradeoff factor.

Proof: Please see Appendix B. ■

$$Q_{p,1}=\sum_{j=0}^{J}(-1)^{j}\binom{J}{j}\left[Q\left(\sqrt{2\beta},\sqrt{\frac{2\xi\left(\beta+1\right)}{V_{sj}}}\right)\right]^{j}\Lambda_1\sum_{t_1=1}^{T_1}\sqrt{\tau_{1,1}}^{\varphi_p+1}\sqrt{1-x_{t_1}^2}\left(1+x_{t_1}\right)^{\varphi_p}e^{-\frac{\left(1+x_{t_1}\right)\sqrt{\tau_{1,1}}}{2\phi_p}}$$
$$\times\left[1-Q\left(\sqrt{2\beta},\left(\frac{\left(1-x_{t_1}\right)}{2}\sqrt{\tau_{1,1}}\right)\sqrt{\frac{2\left(\beta+1\right)}{V_{sp}}}\right)\right], \tag{19}$$

$$Q_{p,2}=\sum_{j=0}^{J}(-1)^{j}\binom{J}{j}\left[Q\left(\sqrt{2\beta},\sqrt{\frac{2\xi\left(\beta+1\right)}{V_{sj}}}\right)\right]^{j}\Lambda_2\sum_{t_2=0}^{T_2}\sqrt{1-x_{t_2}^2}\left(1+x_{t_2}\right)^{\varphi_p}\sum_{p=1}^{P}H_p\Phi^{\varphi_p+1}e^{-\frac{\left(1+x_{t_2}\right)\Phi}{2\phi_p}}$$
$$\times\left[1-Q\left(\sqrt{2\beta},\left(\frac{\left(1-x_{t_2}\right)}{2}\Phi\right)\sqrt{\frac{2\left(\beta+1\right)}{V_{sp}}}\right)\right], \tag{20}$$

$$Q_{p,3}=1-\Lambda_3\sum_{t_3=1}^{T_3}\sqrt{1-x_{t_3}^2}\left(1+x_{t_3}\right)^{\varphi_p}\frac{\pi\xi}{2E}\sum_{e=1}^{E}\sqrt{1-x_e^2}\sqrt{\tau_{1,2}\Phi_e}^{\varphi_p+1}e^{-\frac{\left(1+x_{t_3}\right)\sqrt{\tau_{1,2}\Phi_e}}{2\phi_p}}\frac{J\left(\beta+1\right)}{V_{sj}e^{\beta}}e^{-\frac{\Phi_e(\beta+1)}{V_{sj}}}$$
$$\times\left[1-Q\left(\sqrt{2\beta},\left(\frac{\left(1-x_{t_3}\right)}{2}\sqrt{\tau_{1,2}\Phi_e}\right)\sqrt{\frac{2\left(\beta+1\right)}{V_{sp}}}\right)\right]I_0\left(2\sqrt{\frac{\Phi_e\beta\left(\beta+1\right)}{V_{sj}}}\right)\left[1-Q\left(\sqrt{2\beta},\sqrt{\frac{2\Phi_e\left(\beta+1\right)}{V_{sj}}}\right)\right]^{J-1}, \tag{21}$$

$$Q_{p,4}=1-\Lambda_4\sum_{t_4=1}^{T_4}\sqrt{1-x_{t_4}^2}\left(1+x_{t_4}\right)^{\varphi_p}\frac{\pi\xi}{2H}\sum_{h=1}^{H}\sqrt{1-x_h^2}\frac{J\left(\beta+1\right)}{V_{sj}e^{\beta}}e^{-\frac{\Phi_h(\beta+1)}{V_{sj}}}I_0\left(2\sqrt{\frac{\Phi_h\beta\left(\beta+1\right)}{V_{sj}}}\right)$$
$$\times\left[1-Q\left(\sqrt{2\beta},\sqrt{\frac{2\Phi_h\left(\beta+1\right)}{V_{sj}}}\right)\right]^{J-1}\sum_{p_2=1}^{P_2}H_{p_2}\sqrt{\tau_{2,2}\omega\rho_{th}\Omega_{ip}y_{p_2}+\tau_{2,2}\Phi_h}^{\varphi_p+1}e^{-\frac{\left(1+x_{t_4}\right)\sqrt{\tau_{2,2}\omega\rho_{th}\Omega_{ip}y_{p_2}+\tau_{2,2}\Phi_h}}{2\phi_p}}$$
$$\times\left[1-Q\left(\sqrt{2\beta},\left(\frac{\left(1-x_{t_4}\right)}{2}\sqrt{\tau_{2,2}\omega\rho_{th}\Omega_{ip}y_{p_2}+\tau_{2,2}\Phi_h}\right)\sqrt{\frac{2\left(\beta+1\right)}{V_{sp}}}\right)\right], \tag{22}$$

$$Q_{p,5}=\sum_{j=0}^{J}(-1)^{j}\binom{J}{j}\left[Q\left(\sqrt{2\beta},\sqrt{\frac{2\xi\left(\beta+1\right)}{V_{sj}}}\right)\right]^{j}\sum_{t_5=0}^{T_5}\frac{\pi\tau_1\left(\beta+1\right)\sqrt{1-x_{t_5}^2}}{2T_5V_{sp}e^{\beta}\Gamma\left(\varphi_p+1\right)}\left(1+x_{t_5}\right)e^{-\frac{\tau_1\left(1+x_{t_5}\right)^2(\beta+1)}{4V_{sp}}}$$
$$\times I_0\left(\left(1+x_{t_5}\right)\sqrt{\frac{\tau_1\beta\left(\beta+1\right)}{V_{sp}}}\right)\gamma\left(\varphi_p+1,\frac{\sqrt{\tau_1}\left(1-x_{t_5}\right)}{2\phi_p}\right), \tag{24}$$

$$Q_{p,6}=1-\sum_{t_6=0}^{T_6}\frac{\pi\tau_2\left(\beta+1\right)\sqrt{1-x_{t_6}^2}}{2T_6V_{sp}e^{\beta}\Gamma\left(\varphi_p+1\right)}\left(1+x_{t_6}\right)\frac{\pi\xi}{2E_2}\sum_{e_2=1}^{E_2}\sqrt{1-x_{e_2}^2}\Phi_{e_2}e^{-\frac{\tau_2x\left(1+x_{t_6}\right)^2(\beta+1)}{4V_{sp}}}\frac{J\left(\beta+1\right)}{V_{sj}e^{\beta}}e^{-\frac{\Phi_{e_2}(\beta+1)}{V_{sj}}}$$
$$\times I_0\left(\left(1+x_{t_6}\right)\sqrt{\frac{\tau_2\Phi_{e_2}\beta\left(\beta+1\right)}{V_{sp}}}\right)I_0\left(2\sqrt{\frac{\Phi_{e_2}\beta\left(\beta+1\right)}{V_{sj}}}\right)\gamma\left(\varphi_p+1,\frac{\sqrt{\tau_2\Phi_{e_2}}\left(1-x_{t_6}\right)}{2\phi_p}\right)$$
$$\times\left[1-Q\left(\sqrt{2\beta},\sqrt{\frac{2\Phi_{e_2}\left(\beta+1\right)}{V_{sj}}}\right)\right]^{J-1}, \tag{25}$$

C. OP of the STAR-RIS-OMA network

Different from the STAR-RIS-NOMA network, the SIC scheme is not carried out in the STAR-RIS-OMA network, in which two time phases are included in it. In each time phase, the UAV communicates with a secondary vehicle user. As long as the instantaneous SNR of each SU exceeds the corresponding target SNR, the transmission is successful. Therefore, the OP of SU_u can be represented as

$$P_u^{OMA} = \Pr\left(\gamma_u^{OMA} < \gamma_u^{th}\right). \tag{29}$$

With the similar derivations above, the final expressions of OP for SU_u in the STAR-RIS-OMA network are provided as follows.

Theorem 4. *Considering the Rician fading, the exact expressions of OP for SU_p and SU_q in STAR-RIS-OMA network are represented as* (30) *and* (31)*, respectively, where* $\tau_{3,1} = \frac{\gamma_p^{th}}{\rho_{\max}}$, $\tau_{3,2} = \frac{\gamma_p^{th}}{\rho_{th}}$, $\tau_{4,1} = \frac{\gamma_q^{th}}{\rho_{\max}}$, $\tau_{4,2} = \frac{\gamma_q^{th}}{\rho_{th}}$, $\Phi_m = \frac{(x_m+1)\xi}{2}$, $m = \{e_3, u_2, u_3, u_4\}$, $x_m = \cos\left(\frac{2m-1}{2M}\pi\right)$, $M = \{E_3, U_2, U_3, U_4\}$ *is the Chebyshev tradeoff factor.*

Proof: Similar to the derivation processes of $Q_{p,1}$ and $Q_{p,3}$ in Appendix A, the OP of SU_p for STAR-RIS-OMA is obtained. With the homologous derivations of Appendix B, we can get the OP of SU_q for STAR-RIS-OMA. To make the article more concise, the specific processes are omitted here. ■

D. Asymptotic OP and Diversity Order

In this subsection, the asymptotic OP of secondary vehicle users in different cases at high SNRs is derived. To obtain inherent insights, we also analyze diversity orders to appraise the outage performance of our considered system. The definition of the asymptotic OP is given by

$$P_{out}^{\infty}(\rho_s) = \lim_{\rho_s \to \infty} G\left(\frac{1}{\rho_s}\right)^D. \tag{32}$$

where G is the code gain and D is the diversity order.

Corollary 1. *When $\rho_s \to \infty$, the asymptotic OP of SU_p with ipSIC for STAR-RIS-NOMA can be expressed as*

$$\begin{aligned} P_{p,ipSIC}^{\infty} = {} & Q_{p,1}^{\infty} + Q_{p,2}^{\infty} + Q_{p,3^{\infty}} + Q_{p,4}^{\infty} \\ & - Q_{p,1}^{\infty} Q_{p,2}^{\infty} - Q_{p,3}^{\infty} Q_{p,4}^{\infty}, \end{aligned} \tag{33}$$

where

$$\begin{aligned} Q_{p,1}^{\infty} = {} & \sum_{j=0}^{J} (-1)^j \binom{J}{j} \left[Q\left(\sqrt{2\beta}, \sqrt{\frac{2\xi(\beta+1)}{V_{sj}}}\right)\right]^j \\ & \times \Lambda_1 \sum_{t_1=0}^{T_1} \sqrt{\tau_{1,1}}^{\varphi_p+1} \sqrt{1-x_{t_1}^2} (1+x_{t_1})^{\varphi_p} e^{-\frac{\left(1+x_{t_1}\right)\sqrt{\tau_{1,1}}}{2\phi_p}} \\ & \times \left[1 - Q\left(\sqrt{2\beta}, \left(\frac{(1-x_{t_1})}{2}\sqrt{\tau_{1,1}}\right)\sqrt{\frac{2(\beta+1)}{V_{sp}}}\right)\right], \end{aligned} \tag{34}$$

$$\begin{aligned} Q_{p,2}^{\infty} = {} & \sum_{j=0}^{J} (-1)^j \binom{J}{j} \left[Q\left(\sqrt{2\beta}, \sqrt{\frac{2\xi(\beta+1)}{V_{sj}}}\right)\right]^j \Lambda_2 \\ & \times \sum_{t_2=0}^{T_2} \sqrt{1-x_{t_2}^2} (1+x_{t_2})^{\varphi_p} \sum_{p=1}^{P} \left(\Phi^{1,\infty}\right)^{\varphi_p+1} e^{-\frac{\left(1+x_{t_2}\right)\Phi^{1,\infty}}{2\phi_p}} \\ & \times H_p\left[1 - Q\left(\sqrt{2\beta}, \left(\frac{(1-x_{t_2})}{2}\Phi^{1,\infty}\right)\sqrt{\frac{2(\beta+1)}{V_{sp}}}\right)\right], \end{aligned} \tag{35}$$

$$\begin{aligned} Q_{p,3}^{\infty} = {} & 1 - \Lambda_3 \sum_{t_3=0}^{T_3} \sqrt{1-x_{t_3}^2} (1+x_{t_3})^{\varphi_p} \frac{\pi\xi}{2E} \sum_{e=1}^{E} \sqrt{1-x_e^2} \\ & \times \sqrt{\tau_{1,2}\Phi_e}^{\varphi_p+1} e^{-\frac{\left(1+x_{t_3}\right)\sqrt{\tau_{1,2}\Phi_e}}{2\phi_p}} I_0\left(2\sqrt{\frac{\Phi_e\beta(\beta+1)}{V_{sj}}}\right) \\ & \times \left[1 - Q\left(\sqrt{2\beta}, \left(\frac{(1-x_{t_3})}{2}\sqrt{\tau_{1,2}\Phi_e}\right)\sqrt{\frac{2(\beta+1)}{V_{sp}}}\right)\right] \\ & \times \frac{J(\beta+1)}{V_{sj}e^{\beta}} e^{-\frac{\Phi_e(\beta+1)}{V_{sj}}} \left[1 - Q\left(\sqrt{2\beta}, \sqrt{\frac{2\Phi_e(\beta+1)}{V_{sj}}}\right)\right]^{J-1}, \end{aligned} \tag{36}$$

and

$$\begin{aligned} Q_{p,4}^{\infty} = {} & 1 - \Lambda_4 \sum_{t_4=0}^{T_4} \sqrt{1-x_{t_4}^2} (1+x_{t_4})^{\varphi_p} \frac{\pi\xi}{2H} \sum_{h=1}^{H} J\sqrt{1-x_u^2} \\ & \times \sum_{p_2}^{P_2} \frac{\beta+1}{V_{sj}e^{\beta}} e^{-\frac{\Phi_h(\beta+1)}{V_{sj}} - \frac{\left(1+x_{t_4}\right)\Phi^{2,\infty}}{2\phi_p}} I_0\left(2\sqrt{\frac{\Phi_h\beta(\beta+1)}{V_{sj}}}\right) \\ & \times H_{p_2}\left(\Phi^{2,\infty}\right)^{\varphi_p+1} \left[1 - Q\left(\sqrt{2\beta}, \sqrt{\frac{2\Phi^{2,\infty}(\beta+1)}{V_{sj}}}\right)\right]^{J-1} \\ & \times \left[1 - Q\left(\sqrt{2\beta}, \left(\frac{(1-x_{t_4})}{2}\Phi^{2,\infty}\right)\sqrt{\frac{2(\beta+1)}{V_{sp}}}\right)\right], \end{aligned} \tag{37}$$

with $\Phi^{1,\infty} = \sqrt{\frac{\gamma_p^{th}}{\alpha_p}\omega y_p \Omega_{ip}}$, $\Phi^{2,\infty} = \sqrt{\frac{\gamma_p^{th}}{\alpha_p}\omega \Omega_{ip} y_{p_2}}$.

According to (32), the diversity order of SU_p with ipSIC for STAR-RIS-NOMA is $\min\{0, \frac{\varphi_q+1}{2}\}$, which is affected by the residual interference caused by ipSIC.

Corollary 2. *When $\rho_s \to \infty$, the asymptotic OP of SU_p with pSIC for STAR-RIS-NOMA can be expressed as*

$$P_{p,pSIC}^{\infty} = Q_{p,5}^{\infty} + Q_{p,6}^{\infty} - Q_{p,5}^{\infty} Q_{p,6}^{\infty}, \tag{38}$$

where

$$\begin{aligned} Q_{p,5}^{\infty} = {} & \sum_{j=0}^{J} (-1)^j \binom{J}{j} \left[Q\left(\sqrt{2\beta}, \sqrt{\frac{2\xi(\beta+1)}{V_{sj}}}\right)\right]^j \\ & \times \sum_{t_5=0}^{T_5} \frac{\pi\tau_1(\beta+1)\sqrt{1-x_{t_5}^2}(1+x_{t_5})}{2T_5 V_{sp} e^{\beta}(\varphi_p+1)\Gamma(\varphi_p+1)} e^{-\frac{\tau_1\left(1+x_{t_5}\right)^2(\beta+1)}{4V_{sp}}} \end{aligned}$$

$$P_p^{OMA}=1-\sum_{u_3=0}^{U_3}\frac{\pi\tau_{3,2}\left(\beta+1\right)\sqrt{1-x_{u_3}^2}}{2U_3V_{sp}e^{\beta}\Gamma\left(\varphi_p+1\right)}\left(1+x_{u_3}\right)\frac{\pi\xi}{2E_3}\sum_{e_3=1}^{E_3}\sqrt{1-x_{e_3}^2}\Phi_{e_3}e^{-\frac{\tau_{3,2}x\left(1+x_{u_3}\right)^2\left(\beta+1\right)}{4V_{sp}}}\frac{J\left(\beta+1\right)}{V_{sj}e^{\beta}}e^{-\frac{\Phi_{e_3}\left(\beta+1\right)}{V_{sj}}}$$
$$\times I_0\left(\left(1+x_{u_3}\right)\sqrt{\frac{\tau_2\Phi_{e_3}\beta\left(\beta+1\right)}{V_{sp}}}\right)I_0\left(2\sqrt{\frac{\Phi_{e_3}\beta\left(\beta+1\right)}{V_{sj}}}\right)\gamma\left(\varphi_p+1,\frac{\sqrt{\tau_{3,2}\Phi_{e_3}}\left(1-x_{u_3}\right)}{2\phi_p}\right)$$
$$\times\left[1-Q\left(\sqrt{2\beta},\sqrt{\frac{2\Phi_{e_3}\left(\beta+1\right)}{V_{sj}}}\right)\right]^{J-1}+\sum_{j=0}^{J}\left(-1\right)^j\binom{J}{j}\left[Q\left(\sqrt{2\beta},\sqrt{\frac{2\xi\left(\beta+1\right)}{V_{sj}}}\right)\right]^j\sum_{u_2=0}^{U_2}\frac{\pi\tau_{3,1}\left(\beta+1\right)}{2U_2V_{sp}e^{\beta}}$$
$$\times\frac{\sqrt{1-x_{u_2}^2}}{\Gamma\left(\varphi_p+1\right)}\left(1+x_{t_{u_2}}\right)e^{-\frac{\tau_1\left(1+x_{u_2}\right)^2\left(\beta+1\right)}{4V_{sp}}}I_0\left(\left(1+x_{u_2}\right)\sqrt{\frac{\tau_{3,1}\beta\left(\beta+1\right)}{V_{sp}}}\right)\gamma\left(\varphi_p+1,\frac{\sqrt{\tau_{3,1}}\left(1-x_{u_2}\right)}{2\phi_p}\right),\tag{30}$$

$$P_q^{OMA}=1-\frac{1}{\Gamma\left(\varphi_q+1\right)}\frac{\pi\xi}{2U_4}\sum_{u_4=0}^{U_4}\sqrt{1-x_{u_4}^2}\gamma\left(\varphi_q+1,\frac{\sqrt{\tau_{4,2}\Phi_{u_4}}}{\phi_q}\right)\frac{J\left(\beta+1\right)}{V_{sj}e^{\beta}}e^{-\frac{\Phi_{u_4}\left(\beta+1\right)}{V_{sj}}}I_0\left(2\sqrt{\frac{\Phi_{u_4}\beta\left(\beta+1\right)}{V_{sj}}}\right)$$
$$\times\left[1-Q\left(\sqrt{2\beta},\sqrt{\frac{2\Phi_{u_4}\left(\beta+1\right)}{V_{sj}}}\right)\right]^{J-1}+\sum_{j=0}^{J}\left(-1\right)^j\binom{J}{j}\frac{1}{\Gamma\left(\varphi_q+1\right)}\gamma\left(\varphi_q+1,\frac{\sqrt{\tau_{4,1}}}{\phi_q}\right)^j\left[Q\left(\sqrt{2\beta},\sqrt{\frac{2\xi\left(\beta+1\right)}{V_{sj}}}\right)\right],\tag{31}$$

$$\times I_0\left(\left(1+x_{t_5}\right)\sqrt{\frac{\tau_1\beta\left(\beta+1\right)}{V_{sp}}}\right)\left(\frac{1-x_{t_5}}{2\phi_p}\right)^{\varphi_p+1}{\tau_1}^{\frac{\varphi_p+3}{2}},\tag{39}$$

and

$$Q_{p,6}^{\infty}=1-\sum_{t_6=0}^{T_6}\frac{\pi\left(\beta+1\right)\sqrt{1-x_{t_6}^2}\left(1+x_{t_6}\right)}{2T_6V_{sp}e^{\beta(\varphi_p+1)}\Gamma\left(\varphi_p+1\right)}\frac{\pi\xi}{2E_2}$$
$$\times\sum_{e_2=1}^{E_2}\sqrt{1-x_{e_2}^2}\Phi_{e_2}I_0\left(\left(1+x_{t_6}\right)\sqrt{\frac{\tau_2\Phi_{e_2}\beta\left(\beta+1\right)}{V_{sp}}}\right)$$
$$\times e^{-\frac{\tau_2x\left(1+x_{t_6}\right)^2\left(\beta+1\right)}{4V_{sp}}-\frac{\Phi_{e_2}\left(\beta+1\right)}{V_{sj}}}I_0\left(2\sqrt{\frac{\Phi_{e_2}\beta\left(\beta+1\right)}{V_{sj}}}\right)^{\varphi_p+1}$$
$$\times\frac{J\left(\beta+1\right)}{V_{sj}e^{\beta}}\left[1-Q\left(\sqrt{2\beta},\sqrt{\frac{2\Phi_{e_2}\left(\beta+1\right)}{V_{sj}}}\right)\right]^{J-1}$$
$$\times\left(\frac{\sqrt{\Phi_{e_2}}\left(1-x_{t_6}\right)}{2\phi_p}\right){\tau_2}^{\frac{\varphi_p+3}{2}}.\tag{40}$$

Proof: According to [52, Eq, 8.354.1], one can observe that

$$\gamma\left(\eta,\lambda\right)=\sum_{z=0}^{\infty}\frac{1}{z!\left(\eta+z\right)}\left(\lambda\right)^{\eta+z}.\tag{41}$$

As $\rho_s\to\infty$, we have $\frac{\sqrt{\tau_1}\left(1-x_{t_5}\right)}{2\phi_p}\to 0$, thus we ignore items other than the first item, which is given by

$$\gamma\left(\varphi_p+1,\frac{\sqrt{\tau_1}\left(1-x_{t_5}\right)}{2\phi_p}\right)=\frac{1}{\varphi_p+1}\left(\frac{\sqrt{\tau_1}\left(1-x_{t_5}\right)}{2\phi_p}\right)^{\varphi_p+1}.\tag{42}$$

Combining (42) with (24) and (25), we can get (39) and (40), then the proof is finished. ■

It can be clearly seen that the diversity order of SU_p with pSIC for STAR-RIS-NOMA is $\frac{\varphi_p+3}{2}$.

Corollary 3. *When $\rho_s\to\infty$, the asymptotic OP of SU_q for STAR-RIS-NOMA can be expressed as*

$$P_q^{\infty}=1-\frac{1}{\left(\varphi_q+1\right)\Gamma\left(\varphi_q+1\right)}\left\{\sum_{u_1=0}^{U_1}\sqrt{1-x_{u_1}^2}\frac{\pi\xi J\left(\beta+1\right)}{2U_1V_{sj}e^{\beta}}\right.$$
$$\times\left[1-Q\left(\sqrt{2\beta},\sqrt{\frac{2\Phi_{u_1}\left(\beta+1\right)}{V_{sj}}}\right)\right]^{J-1}e^{-\frac{\Phi_{u_1}\left(\beta+1\right)}{V_{sj}}}{\tau_{1,2}}^{\frac{\varphi_q+1}{2}}$$
$$\times I_0\left(2\sqrt{\frac{\Phi_{u_1}\beta\left(\beta+1\right)}{V_{sj}}}\right)\left(\frac{\sqrt{\Phi_{u_1}}}{\phi_q}\right)^{\varphi_q+1}+\sum_{j=0}^{J}\binom{J}{j}$$
$$\left.\times\left(-1\right)^j\left[Q\left(\sqrt{2\beta},\sqrt{\frac{2\xi\left(\beta+1\right)}{V_{sj}}}\right)\right]^j\left(\frac{1}{\phi_q}\right)^{\varphi_q+1}{\tau_{1,1}}^{\frac{\varphi_q+1}{2}}\right\}.\tag{43}$$

Similar to Corollary 2, we can easily find that the diversity order of SU_q for STAR-RIS-NOMA is $\frac{\varphi_p+1}{2}$.

Corollary 4. *When $\rho_s\to\infty$, the asymptotic OP of SU_p and SU_q for STAR-RIS-OMA can be expressed as* (44) *and* (45)*, respectively.*

Similar to Corollary 2, it can be observed that the diversity orders of SU_p and SU_q in the STAR-RIS-OMA network are $\frac{\varphi_p+3}{2}$ and $\frac{\varphi_p+1}{2}$, respectively.

E. Complexity Analysis

The computational complexity for $Q_{p,1}$, $Q_{p,2}$, $Q_{p,3}$, $Q_{p,4}$, $Q_{p,5}$, $Q_{p,6}$ are $\mathcal{O}\left(JT_1\right)$, $\mathcal{O}\left(JT_2P\right)$, $\mathcal{O}\left(T_3E\right)$, $\mathcal{O}\left(T_4HP_2\right)$, $\mathcal{O}\left(JT_5\right)$, and $\mathcal{O}\left(T_6E_2\right)$, respectively. Hence, we can get the computational complexity of $P_{p,pSIC}$, $P_{p,ipSIC}$, P_p^{OMA} and P_q^{OMA}, which are represented

$$P_p^{OMA,\infty}=1-\sum_{u_3=0}^{U_3}\frac{\pi\left(\beta+1\right)\sqrt{1-x_{u_3}^2}}{2U_3V_{sp}e^{\beta}\left(\varphi_p+1\right)\Gamma\left(\varphi_p+1\right)}\left(1+x_{u_3}\right)\frac{\pi\xi}{2E_3}\sum_{e_3=1}^{E_3}\sqrt{1-x_{e_3}^2}\Phi_{e_3}e^{-\frac{\tau_{3,2}x\left(1+x_{u_3}\right)^2(\beta+1)}{4V_{sp}}-\frac{\Phi_{e_3}(\beta+1)}{V_{sj}}}\frac{J\left(\beta+1\right)}{V_{sj}e^{\beta}}$$
$$\times I_0\left(\left(1+x_{u_3}\right)\sqrt{\frac{\tau_2\Phi_{e_3}\beta\left(\beta+1\right)}{V_{sp}}}\right)I_0\left(2\sqrt{\frac{\Phi_{e_3}\beta\left(\beta+1\right)}{V_{sj}}}\right)\left(\frac{\sqrt{\Phi_{e_3}}\left(1-x_{u_3}\right)}{2\phi_p}\right)^{\varphi_p+1}{\tau_{3,2}}^{\frac{\varphi_p+3}{2}}$$
$$\times\left[1-Q\left(\sqrt{2\beta},\sqrt{\frac{2\Phi_{e_3}\left(\beta+1\right)}{V_{sj}}}\right)\right]^{J-1}+\sum_{j=0}^{J}(-1)^j\binom{J}{j}\left[Q\left(\sqrt{2\beta},\sqrt{\frac{2\xi\left(\beta+1\right)}{V_{sj}}}\right)\right]^j\sum_{u_2=0}^{U_2}\frac{\pi\left(\beta+1\right)}{2U_2V_{sp}e^{\beta}}$$
$$\times\frac{\sqrt{1-x_{u_2}^2}}{\left(\varphi_p+1\right)\Gamma\left(\varphi_p+1\right)}\left(1+x_{t_{u_2}}\right)e^{-\frac{\tau_1\left(1+x_{u_2}\right)^2(\beta+1)}{4V_{sp}}}I_0\left(\left(1+x_{u_2}\right)\sqrt{\frac{\tau_{3,1}\beta\left(\beta+1\right)}{V_{sp}}}\right)\left(\frac{1-x_{u_2}}{2\phi_p}\right)^{\varphi_p+1}{\tau_{3,1}}^{\frac{\varphi_p+3}{2}},\tag{44}$$

$$P_p^{OMA,\infty}=1-\frac{1}{\left(\varphi_q+1\right)\Gamma\left(\varphi_q+1\right)}\left\{\frac{\pi\xi}{2U_4}\sum_{u_4=0}^{U_4}\sqrt{1-x_{u_4}^2}\frac{J\left(\beta+1\right)}{V_{sj}e^{\beta}}e^{-\frac{\Phi_{u_4}(\beta+1)}{V_{sj}}}I_0\left(2\sqrt{\frac{\Phi_{u_4}\beta\left(\beta+1\right)}{V_{sj}}}\right)\left(\frac{\sqrt{\Phi_{u_4}}}{\phi_q}\right)^{\varphi_q+1}\right.$$
$$\left.\times\left[1-Q\left(\sqrt{2\beta},\sqrt{\frac{2\Phi_{u_4}\left(\beta+1\right)}{V_{sj}}}\right)\right]^{J-1}{\tau_{4,2}}^{\frac{\varphi_q+1}{2}}+\sum_{j=0}^{J}(-1)^j\binom{J}{j}\left[Q\left(\sqrt{2\beta},\sqrt{\frac{2\xi\left(\beta+1\right)}{V_{sj}}}\right)\right]^j\left(\frac{1}{\phi_q}\right)^{\varphi_q+1}{\tau_{4,1}}^{\frac{\varphi_q+1}{2}}\right\},\tag{45}$$

as $\mathcal{O}\left(JT_1+JT_2P+T_3E+T_4HP_2\right)$, $\mathcal{O}\left(JT_5+T_6E_2\right)$, $\mathcal{O}\left(U_1+J\right)$, $\mathcal{O}\left(JU_2+U_3E_3\right)$, and $\mathcal{O}\left(J+U_4\right)$, respectively. It worth mentioning that Chebyshev and Laguerre tradeoff factors are dominant which affect the computational complexity. If the Chebyshev/Laguerre tradeoff factors take the same value T/P, the computational complexity of $P_{p,pSIC}$, $P_{p,ipSIC}$, P_p^{OMA} and P_q^{OMA} can be rewritten as $\mathcal{O}\left(JTP+T^2P\right)$, $\mathcal{O}\left(JT+T^2\right)$, $\mathcal{O}\left(J+T\right)$, $\mathcal{O}\left(JT+T^2\right)$, and $\mathcal{O}\left(J+T\right)$, respectively.

IV. Numerical Results

TABLE II
System parameters

Parameter name	Parameter value
Maximum transmitting antenna gain of UAV $G_{s,max}$	48dB
Maximum receive antenna gain of secondary vehicle users $G_{u,max}$	4dB
Receiving antenna diameter of SUs d_u	0.5m
Carrier frequency f	2GHz
Height and UAV/RIS d_x	5km/20m
Distance between the beam center of UAV/RIS and SU_u d_{XY}	1km/1km
Light speed c	3×10^5km/s
3-dB angle ϑ_{3dB}	0.4°
The number of PUs J	10

In this section, numerical results are given to validate the effectiveness of derivations above. As a further advance, the effects of many key parameters, such as the value of residual interference $E\left(|h_{ip}|^2\right)$, the number of transmitting/reflecting elements K, and Rician factor β, on the system performance are revealed, respectively. To balance the accuracy and complexity of the calculation, all Chebyshev and Laguerre tradeoff factors are set as 50 and 100, respectively. According to Section III.E, the computational complexity of $P_{p,pSIC}$, $P_{p,ipSIC}$, P_p^{OMA} and P_q^{OMA} are given by $\mathcal{O}\left(300000\right)$, $\mathcal{O}\left(3000\right)$, $\mathcal{O}\left(60\right)$, $\mathcal{O}\left(3000\right)$, and $\mathcal{O}\left(60\right)$, respectively. The simulation tool is MATLAB 2019a. In general, it is assumed that $R_p^{th}=R_q^{th}=R^{th}$ and the rest parameters are presented in Table I [15], [21]. In addition, the Monte Carlo (MC) simulation is carried out for 10^6 times. For the purpose of comparison, we also utilize the STAR-RIS-OMA network as the benchmark to demonstrate the superiority of our STAR-RIS-NOMA network.

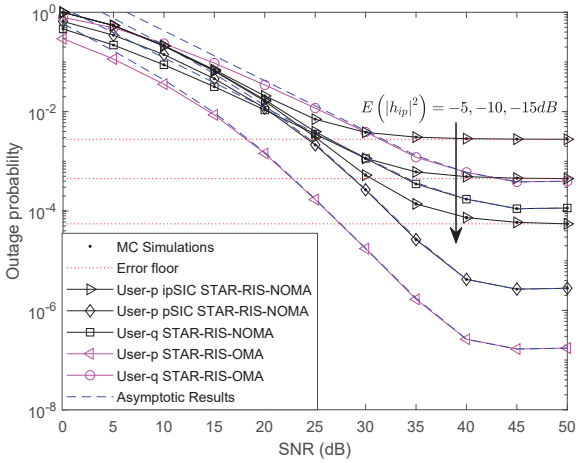

Fig. 2. Outage probability versus SNR with different $E\left(|h_{ip}|^2\right)$.

Fig. 2 shows the outage probability versus SNR with different values of residual interference $E\left(|h_{ip}|^2\right)$, where $\alpha_p = 0.2$, $R^{th} = 1.5b/s/Hz$, $K = 5$, and $\beta = -5dB$. It can be easily found that simulation results are perfectly consistent with our theoretical analysis curves, which indicates that our derivations are correct and accurate. Besides, at high SNR regimes, one can observe that the asymptotic results of secondary vehicle users match with theoretical results in different cases, which enables us to more efficiently analyze the outage performance of the system. However, when the SNR reaches about $40dB$, theoretical curves tend to horizontal straight lines, this is because the interference constraints of PUs restrict the transmit power of the UAV. Furthermore, the OP of SU_p with pSIC outperforms that of SU_q in both the NOMA and OMA network. It is due to the fact that SU_p with pSIC has larger diversity order as derived above. For SU_p with ipSIC, the outage performance improves with the descent of $E\left(|h_{ip}|^2\right)$. With the increase of SNR, OP of SU_p with ipSIC converges to the error floor, which is caused by both interference constraints and residual interference of SIC. Although the outage behavior of SU_p is worse in this case, it is more consistent with the actual communication scenario. Furthermore, the OP of SU_p with pSIC in the NOMA network is inferior to that in the OMA network, while SU_q with STAR-RIS-NOMA has superior outage behavior than with STAR-RIS-OMA. The reason is that SU_p needs to execute the SIC scheme, and more power is allocated to transmit the signals for weaker secondary vehicle user, namely, SU_q. At the same time, it also verifies that the NOMA scheme can provide better user fairness than OMA.

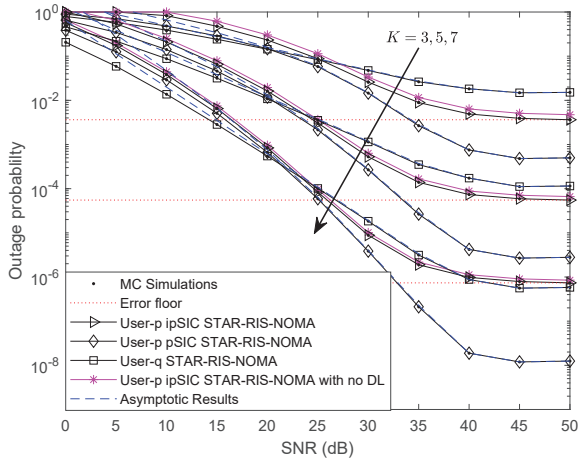

Fig. 3. Outage probability versus SNR with different K.

Fig. 3 illustrates the outage probability versus SNR with different K, where $E\left(|h_{ip}|^2\right) = -15dB$, $\alpha_p = 0.2$, $R^{th} = 1.5b/s/Hz$, and $\beta = -5dB$. As can be observed that OPs of all secondary vehicle users deteriorate with the number of transmitting/reflecting elements. It can be explained by the fact that more RIS elements mean more transmission links. Besides, the slope of curves with pSIC increases with K. This is because their diversity orders are positively correlated with K, which is in line with the analysis in Section III. In addition, it can be clearly seen that the outage behavior of no direct link (DL) topology is weaker than that of our proposed topology. The above analysis enlightens us that for wireless communication systems with high-reliability requirements, the number of RIS elements can be appropriately increased, even at the expense of some complexity.

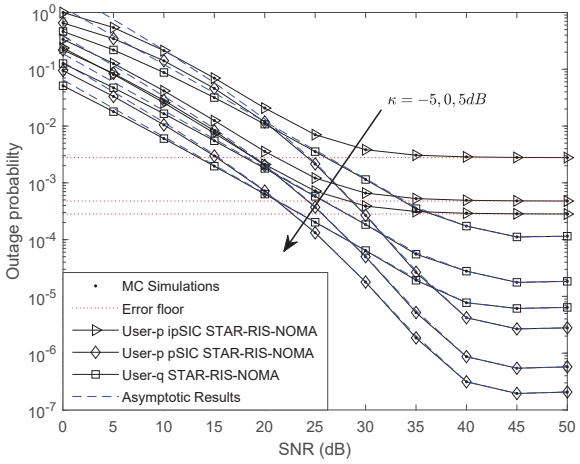

Fig. 4. Outage probability versus SNR with different β.

Fig. 4 depicts the outage probability versus SNR with different β, where $E\left(|h_{ip}|^2\right) = -15dB$, $\alpha_p = 0.2$, $R^{th} = 1.5b/s/Hz$, and $K = 5$. It can be seen that β has a significant impact on the outage behavior of secondary vehicle users. Specifically, the OP of the system declines with the rise of β. The reason is that β determines the line-of-sight components of Rician channels, which is a leading factor of system performance. As a result, it is important to consider the choice of RIS installation location, which has significant impacts on the state of channel fading.

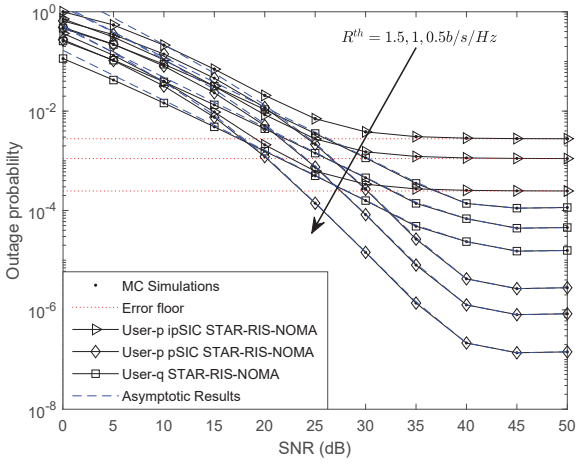

Fig. 5. Outage probability versus SNR with different R^{th}.

Fig. 5 plots the outage probability versus SNR with different R^{th}, where $E\left(|h_{ip}|^2\right) = -15dB$, $\alpha_p = 0.2$, $K = 5$, and $\beta = -5dB$. Predictably, the outage behavior of secondary

vehicle users deteriorates with the increase of the target rate. This phenomenon can be explained that the stricter target rate threshold will make it more difficult for secondary vehicle users to meet the decoding constraints, which will lead to the interruption of communication. Therefore, when pairing users, users with low target rates should be selected as far as possible to ensure that the overall OP of the system is smaller.

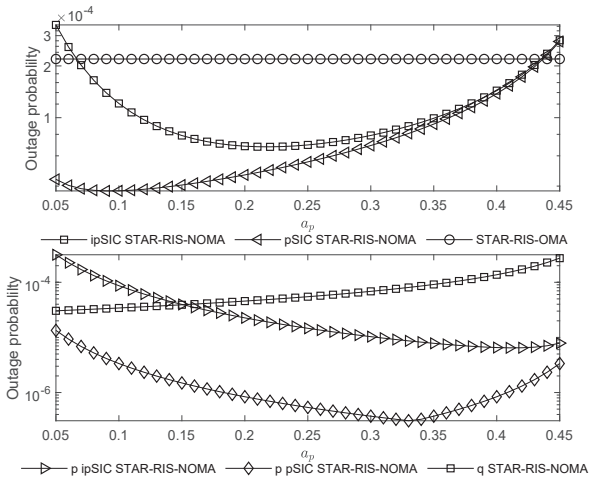

Fig. 6. Outage probability versus power allocation factor in different cases.

Fig. 6 illustrates the outage probability versus power allocation factor in different cases with $E\left(|h_{ip}|^2\right) = -15dB$, $k = 5$, $\rho_s = 25dB$ $R^{th} = 1.5b/s/Hz$, and $\beta = -5dB$. The subfigure on the upper side plots the OP with ipSIC/pSIC for STAR-RIS-NOMA and that for STAR-RIS-OMA versus power allocation factor. It can be clearly seen that OPs for STAR-RIS-NOMA with both ipSIC and pSIC decline first and then enhance with the rise of power allocation factor α_p, which reach the optimal performance at $\alpha_p = 0.23$ and $\alpha_p = 0.1$, respectively. It indicates that the outage performance of the system can be improved by adjusting the power allocation scheme, and the dynamic power allocation problem will be investigated in our future work. Besides, the OP for STAR-RIS-OMA is independent of the power allocation factor. The subfigure on the lower side shows the OP of SU_p with ipSIC/pSIC and that of SU_q versus power allocation factor. For SU_q with both ipSIC and pSIC, OP curves are not monotonous, this is because the SIC process needs to be executed by SU_p. But for q, the increase of α_p leads to the descent of its OP. This inspires us to adjust the power allocation scheme of the system according to the outage demand of each user.

Fig. 7 depicts the system throughput versus SNR with different K, where $E\left(|h_{ip}|^2\right) = -15dB$, $\alpha_p = 0.2$, $R^{th} = 1.5b/s/Hz$, and $\beta = -5dB$. One can observe that the system throughput with pSIC is $0.21b/s/Hz$ higher than that with ipSIC, this is because the system throughput is inversely related to OP. At the same time, the transmission performance for STAR-RIS-NOMA outperforms that for STAR-RIS-OMA ($1.52b/s/Hz$ when SNR is $35dB$), which demonstrates the superiority of our scheme. Similar to Fig. 3, the system throughput increases with K. It is worth mentioning that the

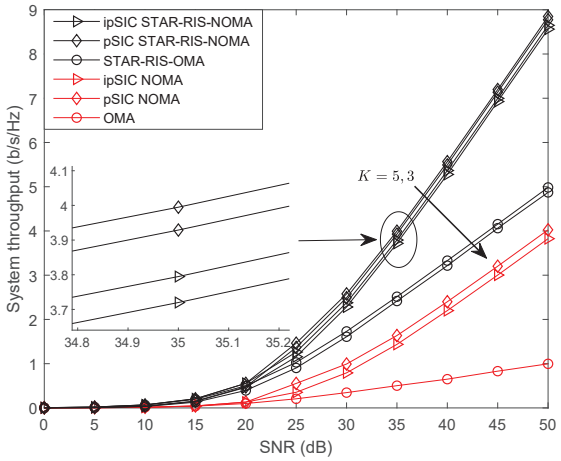

Fig. 7. System throughput versus SNR with different K.

performance of system with STAR-RIS is significantly better than that without STAR-RIS, which confirms that STAR-RIS plays an important role in transmission.

V. Conclusion

In this paper, the performance of a STAR-RIS-empowered non-terrestrial vehicle network was investigated, where CR and NOMA were utilized to enhance SE and connectivity. In particular, the exact expressions of OP for all secondary vehicle users were derived, and ipSIC was considered in our proposed system. To obtain further insights, the asymptotic OPs at high SNRs and diversity orders of all secondary vehicle users were provided. Numerical results demonstrated that STAR-RIS can prominently enhance the performance of wireless communication networks, which can meet different communication demands by increasing/decreasing the number of configurable elements. Besides, CR may limit the transmission power of the SN, but its existence made it possible for the SN to access the authorized spectrum. Compared with OMA, it was confirmed that NOMA can improve user fairness and system throughput. In addition, the outage behavior of secondary vehicle user with ipSIC was weaker than that with pSIC, but pSIC cannot exist in practical communication scenarios. Moreover, the power allocation scheme should be optimized to obtain the enhanced performance of STAR-RIS assisted NOMA network, which is a promising research point. At the same time, the deployment locations of STAR-RIS and imperfect CSI are also worth discussing.

Appendix A
Proof of Theorem 1

By substituting (7) and (8) into (17), OP of SU_p with ipSIC can be re-written as (46), where $\mathcal{Z}=\max\limits_{j=1,2,\cdots,J}|h_{sj}|^2$, $\Xi_R=\left|h_{sp}+\mathbf{h}_{sr}^H\Theta_R\mathbf{h}_{rp}\right|^2$. To derive the final expression of $P_{p,ipSIC}$, the statistical characteristics of $\mathcal{Z}$ and Ξ_R must be obtained.

$$P_{p,ipSIC} = \underbrace{\Pr\left(\rho_{\max} < \frac{\rho_{th}}{\mathcal{Z}}, \Xi_R < \tau_{1,1}\right)}_{Q_{p,1}} + \underbrace{\Pr\left[\rho_{\max} < \frac{\rho_{th}}{\mathcal{Z}}, \Xi_R < \tau_{2,1}\left(\omega\rho_{\max}|h_{ip}|^2 + 1\right)\right]}_{Q_{p,2}}$$
$$+ \underbrace{\Pr\left(\rho_{\max} \geq \frac{\rho_{th}}{\mathcal{Z}}, \Xi_R < \tau_{1,2}\mathcal{Z}\right)}_{Q_{p,3}} + \underbrace{\Pr\left[\rho_{\max} < \frac{\rho_{th}}{\mathcal{Z}}, \Xi_R < \tau_{2,2}\left(\omega\rho_{th}|h_{ip}|^2 + \mathcal{Z}\right)\right]}_{Q_{p,4}}$$
$$- \Pr\left(\rho_{\max} < \frac{\rho_{th}}{\mathcal{Z}}, \Xi_R < \tau_{1,1}\right)\Pr\left[\rho_{\max} < \frac{\rho_{th}}{\mathcal{Z}}, \Xi_R < \tau_{2,1}\left(\omega\rho_{\max}|h_{ip}|^2 + 1\right)\right]$$
$$- \Pr\left(\rho_{\max} \geq \frac{\rho_{th}}{\mathcal{Z}}, \Xi_R < \tau_{1,2}\mathcal{Z}\right)\Pr\left[\rho_{\max} < \frac{\rho_{th}}{\mathcal{Z}}, \Xi_R < \tau_{2,2}\left(\omega\rho_{th}|h_{ip}|^2 + \mathcal{Z}\right)\right], \quad (46)$$

Firstly, the CDF of $\mathcal{Z}$ can be expressed as

$$F_{\mathcal{Z}}(x) = \Pr\left(|h_{s1}|^2 < x\right)\Pr\left(|h_{s2}|^2 < x\right)\cdots\Pr\left(|h_{sJ}|^2 < x\right). \quad (47)$$

According to (13) and the probability transformation formula, the CDF of $|h_{sj}|^2$ is given by

$$F_{|h_{s2}|^2}(x) = 1 - Q\left(\sqrt{2\beta}, \sqrt{\frac{2x(\beta+1)}{V_{sj}}}\right). \quad (48)$$

With the help of [52, Eq. 1.111], and taking (48) into (47), one has

$$F_{\mathcal{Z}}(x) = \sum_{j=0}^{J}(-1)^j \binom{J}{j}\left[Q\left(\sqrt{2\beta}, \sqrt{\frac{2x(\beta+1)}{V_{sj}}}\right)\right]^j. \quad (49)$$

Then the PDF of $\mathcal{Z}$ can be expressed as

$$f_{\mathcal{Z}}(x) = \frac{J(\beta+1)}{V_{sj}e^{\beta}}e^{-\frac{x(\beta+1)}{V_{sj}}}I_0\left(2\sqrt{\frac{x\beta(\beta+1)}{V_{sj}}}\right) \times\left[1 - Q\left(\sqrt{2\beta}, \sqrt{\frac{2x(\beta+1)}{V_{sj}}}\right)\right]^{J-1}. \quad (50)$$

Secondly, let $X_u = \sum_{k=1}^{K} X_u^k$, with the help of (14) as well as [55, Eq, 2.76], the PDF of X_u is given by

$$f_{X_u}(x) = \frac{x^{\varphi_p}}{{\phi_p}^{\varphi_p+1}\Gamma(\varphi_p+1)}e^{-\frac{x}{\phi_p}}. \quad (51)$$

Next, by combining (12) and (51), with some mathematical steps, one has

$$F_{\Xi_R}(\Xi_R) = \int_0^{\sqrt{\Xi_R}} \frac{x^{\varphi_p}}{{\phi_p}^{\varphi_p+1}\Gamma(\varphi_p+1)}e^{-\frac{x}{\phi_p}} \times\left[1 - Q\left(\sqrt{2\beta}, \left(\sqrt{\Xi_R} - x\right)\sqrt{\frac{2(\beta+1)}{V_{sp}}}\right)\right]dx. \quad (52)$$

The above integral is hard to tackle directly, thus Gauss-Chebyshev quadrature is adopted to solve it, which can be expressed as

$$\int_0^z f(x)dx \approx \frac{\pi Z}{2T}\sum_{t=1}^{T} f\left[\frac{(x_t+1)Z}{2}\right]\sqrt{1-x_t^2}, \quad (53)$$

where $x_t = \cos\left(\frac{2t-1}{2T}\pi\right)$, T is the Chebyshev tradeoff factor. Then the PDF of Ξ_R can be expressed as

$$F_{\Xi_R}(\Xi_R) = \Lambda_1\sum_{t_1=1}^{T_1}\sqrt{\Xi_R}^{\varphi_p+1}(1+x_{t_1})^{\varphi_p}e^{-\frac{\left(1+x_{t_1}\right)\sqrt{\Xi_R}}{2\phi_p}} \times\sqrt{1-x_{t_1}^2}\left[1 - Q\left(\sqrt{2\beta}, \left(\frac{(1-x_{t_1})}{2}\sqrt{\Xi_R}\right)\sqrt{\frac{2(\beta+1)}{V_{sp}}}\right)\right]. \quad (54)$$

Then, $Q_{p,1}$ can be re-written as

$$Q_{p,1} = F_{\mathcal{Z}}(\xi)F_{\Xi_R}(\tau_{1,1}). \quad (55)$$

By taking (49) and (54) into (55), we can obtain (19).

Similarly, $Q_{p,2}$ can be re-written as

$$Q_{p,2} = F_{\mathcal{Z}}(\xi)\int_0^{\infty} F_{\Xi_R}\left[\tau_{2,1}\left(\omega\rho_{\max}\Omega_{ip}y + 1\right)\right]\frac{1}{\Omega_{ip}}e^{-\frac{y}{\Omega_{ip}}}dy. \quad (56)$$

By substituting (50) and (54) into (56), we can get (57), (57) contains the indefinite integral, thus we utilize Gauss-Laguerre quadrature to solve it, which is represented as

$$\int_0^{\infty} f(y)e^{-y}dy \approx \sum_{p=1}^{P} H_p f(y_p). \quad (58)$$

Combining (58) with (57), we can get (20).

Next, $Q_{p,3}$ can be re-written as

$$Q_{p,3} = 1 - \int_0^{\xi} F_{\Xi_R}(\tau_{1,2}x)f_{\mathcal{Z}}(x)dx. \quad (59)$$

By taking (50) and (54) into (59), with the help of Gauss-Chebyshev quadrature, one has (21).

Then, $Q_{p,4}$ can be re-written as

$$Q_{p,4} = 1 - \int_0^{\infty}\int_0^{\xi} F_{\Xi_R}\left(\tau_{2,2}\omega\rho_{th}y + \tau_{2,2}x\right)f_{\mathcal{Z}}(x)e^{-y}dxdy. \quad (60)$$

By taking (50) and (54) into (60), with the help of Gauss-Chebyshev and Gauss-Laguerre quadrature, (22) is obtained.

$$Q_{p,2}=\sum_{j=0}^{J}(-1)^{j}\left(\begin{array}{c}J\\ j\end{array}\right)\left[Q\left(\sqrt{2\beta},\sqrt{\frac{2\xi\left(\beta+1\right)}{V_{sj}}}\right)\right]^{j}\left\{\Lambda_2\sum_{t_2=0}^{T_2}\sqrt{1-x_{t_2}^2}(1+x_{t_2})^{\varphi_p}\int_0^{\infty}\frac{\sqrt{\tau_{2,1}\left(\omega\rho_{\max}y+1\right)}^{\varphi_p+1}}{\Omega_{ip}}\right.$$
$$\left.\times\, e^{-\frac{y}{\Omega_{ip}}-\frac{\left(1+x_{t_2}\right)\sqrt{\tau_{2,1}(\omega\rho_{\max}y+1)}}{2\phi_p}}\left[1-Q\left(\sqrt{2\beta},\left(\frac{(1-x_{t_2})}{2}\sqrt{\tau_{2,1}\left(\omega\rho_{\max}y+1\right)}\right)\sqrt{\frac{2\left(\beta+1\right)}{V_{sp}}}\right)\right]\right\}, \tag{57}$$

Finally, by substituting (19), (20), (21), and (22) into (46), the final expression of OP for SU_p with ipSIC (18) is obtained. The proof of Theorem 1 is completed.

Appendix B
Proof of Theorem 3

By taking (9) into (27), one can observe

$$P_q=\underbrace{\Pr\left(\rho_{\max}<\frac{\rho_{th}}{\mathcal{Z}}\right)\Pr\left(\Xi_T<\tau_{1,1}\right)}_{Q_{q,1}}$$
$$+\underbrace{\Pr\left(\rho_{\max}\geq\frac{\rho_{th}}{\mathcal{Z}}\right)\Pr\left(\Xi_T<\tau_{1,2}\mathcal{Z}\right)}_{Q_{q,2}}. \tag{61}$$

Thus the CDF of Ξ_T must be provided. Similar to (51), we can get

$$f_{\Xi_T}\left(x\right)=\frac{x^{\varphi_q}}{{\phi_q}^{\varphi_q+1}\Gamma\left(\varphi_q+1\right)}e^{-\frac{x}{\phi_q}}. \tag{62}$$

By integrating the above equation, the CDF of Ξ_T is obtained as

$$F_{\Xi_T}\left(x\right)=\frac{1}{\Gamma\left(\varphi_q+1\right)}\gamma\left(\varphi_q+1,\frac{\sqrt{x}}{\phi_q}\right). \tag{63}$$

Next, $Q_{q,1}$ can be re-written as

$$Q_{q,1}=F_{\mathcal{Z}}\left(\xi\right)F_{\Xi_T}\left(\tau_{1,1}\right). \tag{64}$$

By taking (49) and (63) into (64), we can get

$$Q_{q,1}=\frac{1}{\Gamma\left(\varphi_q+1\right)}\sum_{j=0}^{J}\left(\begin{array}{c}J\\ j\end{array}\right)(-1)^{j}\gamma\left(\varphi_q+1,\frac{\sqrt{\tau_{1,1}}}{\phi_q}\right)$$
$$\times\left[Q\left(\sqrt{2\beta},\sqrt{\frac{2\xi\left(\beta+1\right)}{V_{sj}}}\right)\right]^{j}. \tag{65}$$

Then, $Q_{q,2}$ can be re-written as

$$Q_{q,2}=1-\int_0^{\xi}F_{\Xi_T}\left(\tau_{1,2}x\right)f_{\mathcal{Z}}\left(x\right)dx. \tag{66}$$

By taking (50) and (63) into (66), with the help of Gauss-Chebyshev quadrature, one has

$$Q_{q,2}=1-\frac{1}{\Gamma\left(\varphi_q+1\right)}\frac{\pi\xi}{2U_1}\sum_{u_1=0}^{U_1}\sqrt{1-x_{u_1}^2}\frac{J\left(\beta+1\right)}{V_{sj}e^{\beta}}e^{-\frac{\Phi_{u_1}(\beta+1)}{V_{sj}}}$$
$$\times\,\gamma\left(\varphi_q+1,\frac{\sqrt{\tau_{1,2}\Phi_{u_1}}}{\phi_q}\right)I_0\left(2\sqrt{\frac{\Phi_{u_1}\beta\left(\beta+1\right)}{V_{sj}}}\right)$$
$$\times\left[1-Q\left(\sqrt{2\beta},\sqrt{\frac{2\Phi_{u_1}\left(\beta+1\right)}{V_{sj}}}\right)\right]^{J-1}. \tag{67}$$

Finally, combining (65) and (67) into (61), the final expression of OP for SU_q, namely, (28) is obtained. The proof of Theorem 3 is completed.

References

[1] G. Pan *et al.*, "On HARQ schemes in satellite-terrestrial transmissions," *IEEE Trans. Wireless Commun.*, vol. 19, no. 12, pp. 7998-8010, Dec. 2020.

[2] G. Pan *et al.*, "Latency versus reliability in LEO mega-constellations: Terrestrial, aerial, or space Relay," *IEEE Trans. Mob. Comput.*, early access, doi: 10.1109/TMC.2022.3168081.

[3] N. Zhao *et al.*, "Caching unmanned aerial vehicle-enabled small-cell networks: Employing energy-efficient methods that store and retrieve popular content," *IEEE Veh. Tech. Mag.*, vol. 14, no. 1, pp. 71-79, Mar. 2019.

[4] F. Zhou *et al.*, "Secrecy performance for RIS-based integrated satellite vehicle networks with a UAV relay and MRC eavesdropping," *IEEE trans. Intell. Veh.*, vol. 8, no. 2, pp. 1676-1685, Feb. 2023.

[5] L. Lv *et al.*, "When NOMA meets multiuser cognitive radio: Opportunistic cooperation and user scheduling," *IEEE Trans. Veh. Tech.*, vol. 67, no. 7, pp. 6679-6684, Jul. 2018.

[6] L. Lv *et al.*, "Cognitive non-orthogonal multiple access with cooperative relaying: A new wireless frontier for 5G spectrum sharing," *IEEE Commun. Mag.*, vol. 56, no. 4, pp. 188-195, Apr. 2018.

[7] X. Yue *et al.*, "Secure communications in a unified non-orthogonal multiple access framework," *IEEE Trans. Wireless Commun.*, vol. 19, no. 3, pp. 2163-2178, Mar. 2020.

[8] Y. Liu *et al.*, "Simultaneous transmission and reflection for 360 coverage by intelligent surfaces," *IEEE Wireless Commun.*, vol. 28, no. 6, pp. 102-109, Dec. 2021.

[9] L. Yang *et al.*, "Outage performance of UAV-assisted relaying systems with RF energy harvesting," *IEEE Commun. Lett.*, vol. 22, no. 12, pp. 2471-2474, Dec. 2018.

[10] L. Yang and M. O. Hasna, "Performance analysis of amplify-and-forward hybrid satellite-terrestrial networks with cochannel interference," *IEEE Trans. Commun.*, vol. 63, no. 12, pp. 5052-5061, Dec. 2015.

[11] K. Guo *et al.*, "Ergodic capacity of NOMA-based overlay cognitive integrated satellite-UAV-terrestrial networks," *Chinese J. Electron.*, vol. 32, no. 2, pp. 273-282, Mar. 2023.

[12] R. Liu *et al.*, "Resource allocation for NOMA-enabled cognitive satellite-UAV-terrestrial networks with imperfect CSI," *IEEE Trans. Cogn. Commun.*, early access, doi: 10.1109/TCCN.2023.3261311.

[13] Y. Ruan *et al.*, "Energy efficient adaptive transmissions in integrated satellite-terrestrial networks with SER constraints," *IEEE Trans. Wireless Commun.*, vol. 17, no. 1, pp. 210-222, Jan. 2018.

[14] Q. Huang *et al.*, "Performance analysis of integrated satellite-terrestrial multiantenna relay networks with multiuser scheduling," *IEEE Trans. Aerosp. Electron. Syst.*, vol. 56, no. 4, pp. 2718-2731, Aug. 2020.

[15] K. Guo *et al.*, "On the performance of LMS communication with hardware impairments and interference," *IEEE Trans. Commun.*, vol. 67, no. 2, pp. 1490-1505, Feb. 2019.

[16] K. Guo *et al.*, "On the performance of RIS-assisted integrated satellite-UAV-terrestrial networks with hardware impairments and interference," *IEEE Wireless Commun. Lett.*, vol. 11, no. 1, pp. 131-135, Jan. 2022.

[17] G. Pan *et al.*, "Performance analysis and optimization of cooperative satellite-aerial-terrestrial systems," *IEEE Trans. Wireless Commun.*, vol. 19, no. 10, pp. 6693-6707, Oct. 2020.

[18] K. Guo *et al.*, "Physical layer security for multiuser satellite communication systems with threshold-based scheduling scheme," *IEEE Trans. Veh. Tech.*, vol. 69, no. 5, pp. 5129-5141, May 2020.

[19] K. Guo *et al.*, "On the secrecy performance of NOMA-based integrated satellite multiple-terrestrial relay networks with hardware impairments," *IEEE Trans. Veh. Tech.*, vol. 70, no. 4, pp. 3661-3676, Apr. 2021.

[20] K. An *et al.*, "Secure transmission in cognitive satellite terrestrial networks," *IEEE J. Sel. Areas Commun.*, vol. 34, no. 11, pp. 3025-3037, Nov. 2016.
[21] R. Liu *et al.*, "NOMA-based integrated satellite-terrestrial relay networks under spectrum sharing environment," *IEEE Wireless Commun. Lett.*, vol. 10, no. 6, pp. 1266-1270, Jun. 2021.
[22] Y. Ruan *et al.*, "Power allocation in cognitive satellite-vehicular networks from energy-spectral efficiency tradeoff perspective," *IEEE Trans. Cogn. Commun.*, vol. 5, no. 2, pp. 318-329, Jun. 2019.
[23] X. Li *et al.*, "Physical layer security of cognitive ambient backscatter communications for green Internet-of-Things", *IEEE Trans. Green Commun. Netw.*, vol. 5, no. 3, pp. 1066-1076, Sep. 2021.
[24] P. K. Sharma *et al.*, "Performance analysis of overlay spectrum sharing in hybrid satellite-terrestrial systems with secondary network selection," *IEEE Trans. Wireless Commun.*, vol. 16, no. 10, pp. 6586-6601, Oct. 2017.
[25] V. Singh *et al.*, "Performance analysis of hardware-impaired overlay cognitive satellite-terrestrial networks with adaptive relaying protocol," *IEEE Syst. J.*, vol. 15, no. 1, pp. 192-203, Mar. 2021.
[26] G. Li *et al.*, "Channel-aware power allocation and decoding order in overlay cognitive NOMA networks," *IEEE Trans. Veh. Tech.*, vol. 69, no. 6, pp. 6511-6524, Jun. 2020.
[27] X. Li, et al., "Cognitive AmBC-NOMA IoV-MTS networks with IQI: Reliability and security analysis," *IEEE trans. Intell. Transp. Syst.*, vol. 24, no. 2, pp. 2596-2607, Feb. 2023.
[28] Y. Ruan *et al.*, "Energy efficient power control for cognitive multibeam-satellite terrestrial networks with poisson distributed users," *IEEE Trans. Cogn. Commun.*, vol. 8, no. 2, pp. 964-974, Jun. 2022.
[29] Z. Lin *et al.*, "Robust secure beamforming for wireless powered cognitive satellite-terrestrial networks", *IEEE Trans. Cogn. Commun.*, vol. 7, no. 2, pp. 567-580, Jun. 2021.
[30] X. Li *et al.*, "Residual transceiver hardware impairments on cooperative NOMA networks," *IEEE Trans. Wireless Commun.*, vol. 19, no. 1, pp. 680-695, Jan. 2020.
[31] L. Lv *et al.*, "Secure non-orthogonal multiple access: An interference engineering perspective," *IEEE Netw.*, vol. 35, no. 4, pp. 278-285, Jul. 2021.
[32] X. Yue *et al.*, "Outage behaviors of NOMA-based satellite network over shadowed-Rician fading channels," *IEEE Trans. Veh. Tech.*, vol. 69, no. 6, pp. 6818-6821, Jun. 2020.
[33] R. Liu *et al.*, "NOMA-based overlay cognitive integrated satellite-terrestrial relay networks with secondary network selection," *IEEE Trans. Veh. Tech.*, vol. 71, no. 2, pp. 2187-2192, Feb. 2022.
[34] X. Li *et al.*, "Hardware impaired ambient backscatter NOMA systems: Reliability and security," *IEEE Trans. Commun.*, vol. 69, no. 4, pp. 2723-2736, Apr. 2021.
[35] X. Li *et al.*, "Cooperative wireless-powered NOMA relaying for B5G IoT networks with hardware impairments and channel estimation errors," *IEEE Internet Things J.*, vol. 8, no. 7, pp. 5453-5467, Apr. 2021.
[36] N. Zhao *et al.*, "Joint trajectory and precoding optimization for UAV-assisted NOMA networks," *IEEE Trans. Commun.*, vol. 67, no. 5, pp. 3723-3735, May 2019.
[37] V. Singh *et al.*, "Exploiting cache-free/cache-aided TWR-NOMA in cognitive hybrid satellite-terrestrial networks," *IEEE Trans. Veh. Tech.*, vol. 71, no. 2, pp. 1778-1793, Feb. 2022.
[38] K. Guo *et al.*, "NOMA-based cognitive satellite terrestrial relay network: Secrecy performance under channel estimation errors and hardware impairments," *IEEE Internet Things J.*, vol. 9, no. 18, pp. 17334-17347, Sep. 2022.
[39] L. Yang *et al.*, "Performance analysis of RIS-aided networks with co-channel interference," *IEEE Commun. Lett.*, vol. 26, no. 1, pp. 49-53, Jan. 2022.
[40] L. Yang *et al.*, "On the performance of RIS-assisted dual-hop UAV communication systems," *IEEE Trans. Veh. Tech.*, vol. 69, no. 9, pp. 10385-10390, Sep. 2020.
[41] L. Yang *et al.*, "Performance analysis of RIS-assisted UAV communication systems," *IEEE Trans. Veh. Tech.*, vol. 71, no. 8, pp. 9078-9082, Aug. 2022.
[42] X. Yue *et al.*, "Performance analysis of intelligent reflecting surface assisted NOMA networks," *IEEE Trans. Wireless Commun.*, vol. 21, no. 4, pp. 2623-2636, Apr. 2022.
[43] Z. Liu *et al.*, "Performance analysis of reconfigurable intelligent surface assisted two-way NOMA networks," *IEEE Trans. Veh. Tech.*, vol. 71, no. 12, pp. 13091-13104, Dec. 2022.
[44] M. Diamanti, E. E. Tsiropoulou and S. Papavassiliou, "The joint power of NOMA and reconfigurable intelligent surfaces in SWIPT networks," *2021 IEEE 22nd International Workshop on Signal Processing Advances in Wireless Communications (SPAWC)*, 2021, pp. 621-625.
[45] Y. Sun *et al.*, "Outage constrained robust beamforming optimization for multiuser IRS-assisted anti-jamming communications with incomplete information," *IEEE Internet Things J.*, vol. 9, no. 15, pp. 13298-13314, Aug. 2022.
[46] Y. Sun *et al.*, "RIS-assisted robust hybrid beamforming against simultaneous jamming and eavesdropping attacks," *IEEE Trans. Wireless Commun.*, vol. 21, no. 11, pp. 9212-9231, Nov. 2022.
[47] X. Yue *et al.*, "Simultaneously transmitting and reflecting reconfigurable intelligent surface assisted NOMA Networks," *IEEE Trans. Wireless Commun.*, vol. 22, no. 1, pp. 189-204, Jan. 2023.
[48] X. Li *et al.*, "Enhancing secrecy performance for STAR-RIS NOMA networks," *IEEE Trans. Veh. Tech.*, vol. 72, no. 2, pp. 2684-2688, Feb. 2023.
[49] H. Niu *et al.*, "Weighted sum rate optimization for STAR-RIS-assisted MIMO system," *IEEE Trans. Veh. Tech.*, vol. 71, no. 2, pp. 2122-2127, Feb. 2022
[50] H. Niu *et al.*, "Simultaneous transmission and reflection reconfigurable intelligent surface assisted secrecy MISO networks," *IEEE Commun. Lett.*, vol. 25, no. 11, pp. 3498-3502, Nov. 2021.
[51] D. A. Shnidman, "The calculation of the probability of detection and the generalized marcum Q-function," *IEEE Trans. Inf. Theory*, vol. 35, pp. 389-400, Mar. 1989.
[52] I. S. Gradshteyn and I. M. Ryzhik, *Table of Intergals, Series, and Products.*, 7th ed. Academic Press, Amsterdam, The Netherlands, 2007.
[53] Y. Zhu *et al.*, "Outage probability of Rician fading relay channels," *IEEE Trans. Veh. Tech.*, vol. 57, no. 4, pp. 2648-2652, Jul. 2008.
[54] M. K. Simon, *Probability distributions involving gaussian random variables.*, Springer, New York, 2006.
[55] V. K. S. Primak and V. Lyandres, *Stochastic methods and their applications to communications: Stochastic differential equations approach.*, West Sussex, U.K.: Wiley, 2004.

Kefeng Guo received his B.S. degree from Beijing Institute of Technology, Beijing, China in 2012, and the Ph.D. degree in Army Engineering University, Nanjing, China in 2018. He is a Lecturer in School of Space Information, Space Engineering University. He is also the associate professor in the College of Electronic and Information Engineering, Nanjing University of Aeronautics and Astronautics. He has authored or coauthored nearly 70 research papers in international journals and conferences. His research interests focus on cooperative relay networks, MIMO communications systems, multiuser communication systems, satellite communication, hardware impairments, cognitive radio, NOMA technology and physical layer security. He was a recipient of exemplary Reviewer for **IEEE Transactions on Communications** in 2022. He was the recipient of the Outstanding Ph.D. Thesis Award of Chinese Institute of Command and Control in 2020. He also was the recipient of the Excellent Ph.D. Thesis Award of Jiangsu Province, China in 2020. He also serves as an Editor on the Editorial Board for the **EURASIP Journal on Wireless Communications and Networking**. He was the Guest Editor for the special issue on Integration of Satellite-Aerial-Terrestrial Networks of **Sensors** , also the Guest Editor for the special issue on Recent Advances and Challenges of Satellite and Aerial Communication Networks of **Electronics** .

Dr. Guo has been the TPC member of many IEEE sponsored conferences, such as IEEE ICC, IEEE GLOBECOM and IEEE WCNC.

Rui Liu received his B.S. degree from Space Engineering University, Beijing, China, in 2019. He is currently working toward his Ph.D. degree in Space Engineering University. His research interests focus on satellite-terrestrial networks, cognitive radio systems, wireless communication systems and multiuser communication system. He has authored or co authored over 20 papers in international journals and conferences. He was the TPC member for the ISCT workshop.

Mamoun Alazab (Senior Member, IEEE) is a full Professor at the Faculty of Science and Technology, and the Inaugural Director of the NT Academic Centre for Cyber Security and Innovation (ACCI) at Charles Darwin University, Australia. He is a cyber security researcher and practitioner with industry and academic experience. His research is multidisciplinary and focuses on cyber security, data analytics and digital forensics with a focus on cybercrime detection and prevention. He presented more than 130 invited and keynotes talks in an academic, industrial and government and convened and chaired more than 200 conferences and workshops. He serves as the Associate Editor of IEEE Transactions on Computational Social Systems, IEEE Transactions on Network and Service Management (TNSM), ACM Digital Threats: Research and Practice, Digital Investigation, Complex & Intelligent Systems.

Rutvij H. Jhaveri (Senior Member, IEEE) is an experienced educator and researcher working in the Department of Computer Science & Engineering, Pandit Deendayal Energy University, Gandhinagar, India. He conducted his Postdoctoral Research at Delta-NTU Corporate Lab for Cyber-Physical Systems, Nanyang Technological University, Singapore. He completed his PhD in Computer Engineering in 2016. In 2017, he was awarded with prestigious Pedagogical Innovation Award by Gujarat Technological University. Currently, he is co-investigating a funded project from GUJCOST. He was ranked among top 2% scientists around the world in 2022 and 2021. He has 2600+ Google Scholar citations with h-index 26. He is an editorial board member in various journals of repute including IEEE Transactions on Industrial Informatics and Scientific Reports. He also serves as a reviewer in several international journals and also as an advisory/TPC member in renowned international conferences. He authored 135+ articles including the IEEE/ACM Transactions and flagship IEEE/ACM conferences. Moreover, he has several national and international patents and, copyrights to his name. He also possesses memberships of various technical bodies such as ACM, CSI, ISTE and others. He is a member of the Advisory Board in Symbiosis Institute of Digital and Telecom Management, and other reputed universities since 2022. He is an editorial board member in several Springer and Hindawi journals. He also served as a committee member in "Smart Village Project" - Government of Gujarat, at the district level during the year 2017. His research interests are Cyber Security, IoT systems, SDN and Smart Healthcare.

Xingwang Li (S'12-M'15-SM'20) received the M. Sc. and Ph. D. degrees from University of Electronic Science and Technology of China and Beijing University of Posts and Telecommunications in 2010 and 2015. From 2010 to 2012, he worked at Comba Telecom Ltd. In Guangzhou China, as an engineer. He spent one year from 2017 to 2018 as a visiting scholar at Queen's University Belfast, Belfast, UK. He is currently an Associated Professor with the School of Physics and Electronic Information Engineering, Henan Polytechnic University, Jiaozuo China. His research interests span wireless communication, intelligent transport system, artificial intelligence, Internet of things.

Dr. Li has served as many TPC members, such as the IEEE Globecom, IEEE ICC, IEEE WCNC, IEEE VTC, IEEE ICCC etc. He has also served as the Co-Chair for the IEEE/IET CSNDSP 2020 of the Green Communications and Networks Track. He also serves as an Editor on the Editorial Board for IEEE Transactions on Intelligent Transportation Systems, IEEE Transactions on Vehicular Technology, IEEE Systems Journal, Physical Communication. He was the Guest Editor for the special issue on Computational Intelligence and Advanced Learning for Next-Generation Industrial IoT of IEEE Transactions on Network Science and Engineering, "Recent Advances in Physical Layer Technologies for 5G-Enabled Internet of Things" of the Wireless Communications and Mobile Computing.

Mingfu Zhu received the B.Sc. degree from Tianjin University, Tianjin, China, in 2000, the M.Sc. degree from East China Normal University, Shanghai, China, in 2004, and the Ph.D. degree from the University of California, Los Angeles (UCLA), Los Angeles, CA, USA, in 2007. From 2011 to 2013, he was with Mayyard Photoelectric Technology Company Ltd., Ningbo, China, as the Executive Director. Since 2013, he has been the Founder and the Chairperson of Hebi National Optoelectronics Technology Company Ltd., Hebi, China. He is currently the Chairperson of Henan Chuangzhi Technology Company Ltd., Henan, China, and the General Manager of Henan Chuitian Technology Company Ltd., Hebi. He is also working at the College of Computer Science and Technology, Henan Polytechnic University, Jiaozuo, China. His research interests include chip packaging and intelligent light development and manufacturing. With innovative ideas, intelligent lights are used to build intraocular lens (IOL), integrate IOL into IoT, and upgrade to 5G IoT. By building scientific research platforms and manufacturing bases, the 5G industry ecosystem is built to interact with upstream and downstream enterprises.

Dr. Zhu has served as a member of Henan Chinese Peoples Political Consultative Conference (CPPCC). His main awards and achievements include the excellent builder for the socialist cause with Chinese characteristics, special government allowance under the State Council, and leading talents in Science and Technology Innovation of National Ten Thousand Talents Plan. He has served as the Vice President of the Henan Euro-American Alumni Association. He is also the President of the Henan Alumni Association of Tianjin University and the Director of the Henan Mechanical Engineering Society.